HYPEBOY: GENERATIVE SELF-SUPERVISED REPRESENTATION LEARNING ON HYPERGRAPHS

Anonymous authors
Paper under double-blind review

ABSTRACT

Hypergraphs are marked by complex topology, expressing higher-order interactions among multiple nodes with hyperedges, and better capturing the topology is essential for effective representation learning. Recent advances in generative self-supervised learning (SSL) suggest that hypergraph neural networks (HNNs) learned from generative self-supervision have the potential to effectively encode the complex hypergraph topology. Designing a generative SSL strategy for hypergraphs, however, is not straightforward. Questions remain with regard to its generative SSL task, connection to downstream tasks, and empirical properties of learned representations. In light of the promises and challenges, we propose a novel generative SSL strategy for hypergraphs. We first present a generative SSL task on hypergraphs, *hyperedge filling*, and highlight its theoretical connection to node classification. Based on the generative SSL task, we propose a hypergraph SSL method, HYPEBOY. HYPEBOY learns effective general-purpose hypergraph representations, outperforming 15 baseline methods across 11 benchmark datasets. To our knowledge, this is the first study on generative SSL on hypergraphs, and we demonstrate its theoretical and empirical strengths for hypergraph representation learning.

1 INTRODUCTION

Many real-world interactions occur among multiple entities, such as online group discussions on social media, academic collaboration of researchers, and joint item purchases. Representing such higher-order interactions with an ordinary graph can cause topological information loss (Dong et al., 2020). Thus, hypergraphs have emerged as an effective tool for representing high-order interactions in various domains, including recommender systems (Xia et al., 2022; Yu et al., 2021), financial analysis (Sawhney et al., 2021; 2020), and drug analysis (Ruan et al., 2021; Saifuddin et al., 2023).

For representation learning on such a complex topology, hypergraph neural networks (HNNs) have been developed. Training HNNs has primarily relied on task-related label supervision, such as external node labels. However, simply learning from external supervision may limit HNNs from capturing more complex patterns in hypergraph topology. Incorporating self-supervision related to topology, hence, can substantially improve HNNs' representation learning.

Particularly, *generative self-supervised learning* (SSL) holds promise for effective hypergraph representation learning. Generative SSL has recently shown remarkable success in encoding complex patterns in multiple domains. GPT (OpenAI, 2023) in natural language processing and Masked Autoencoder (He et al., 2022) in computer vision are notable examples. With generative self-supervision, HNNs may encode complex topology more effectively, leading to improved representation learning.

However, designing a generative SSL strategy for hypergraphs is not straightforward. First, questions remain unanswered for generative *SSL tasks*: (1.a) What should be the target generative SSL task for HNNs? (1.b) How does the generative SSL task relate to downstream tasks (e.g., node classification with external labels)? Second, even after determining the task, details of the *SSL method* (based on the task) remain unspecified. (2.a) What empirical properties should the method aim to satisfy? (2.b) How can it achieve effective general-purpose hypergraph representations? Moreover, if not carefully designed, the generative SSL strategy can suffer from severe computational burden, as the number of potential hyperedges approaches 2^n, where n denotes the number of nodes.

In light of the promises and challenges, we systematically investigate and propose a hypergraph generative SSL strategy. To our knowledge, this is the first study on generative SSL for hypergraphs. Our contributions and the rest of the paper are organized as follows:

- **SSL Task**: We formulate a novel generative SSL task, *hyperedge filling*, for hypergraph representation learning. Notably, we establish its theoretical connections to node classification (Section 3).
- **SSL Method**: Based on the hyperedge filling task, we propose HYPEBOY, a novel hypergraph SSL method. HYPEBOY is designed to satisfy desirable properties of hypergraph SSL, mitigating (1) over-emphasized proximity, (2) dimensional collapse, and (3) non-uniformity/-alignment of learned representations (Section 4).
- **Experiments**: We demonstrate that HYPEBOY learns effective general-purpose hypergraph representations. It significantly outperforms SSL-based HNNs in both node classification and link prediction across 11 benchmark hypergraphs (Section 5; code and datasets are available at `link`).

2 RELATED WORK

In this section, we review the literature on hypergraph neural networks and self-supervised learning.

Hypergraph neural networks (HNNs). HNNs learn hypergraph representation. Converting hyperedges into cliques (fully connected subgraphs) allows graph neural networks to be applied to hypergraphs (Feng et al., 2019; Yadati et al., 2019). Such conversion, however, may result in topological information loss, since high-order interactions (hyperedges) are reduced to pair-wise interactions (edges). As such, most HNNs pass messages through hyperedges to encode hypergraphs. Some notable examples include HNHN (Dong et al., 2020) with a hyperedge encoder, UniGNN (Huang & Yang, 2021) with generalized message passing for graphs and hypergraphs, AllSet (Chien et al., 2022) with a set encoder, ED-HNN (Wang et al., 2023a) with permutation-equivariant diffusion operators, and PhenomNN (Wang et al., 2023b) with hypergraph-regularized energy functions. ***Note***: The discussed HNNs are hypergraph encoders, with no dedication to a particular loss objective. We clarify that our interest is in designing a generative SSL strategy for hypergraphs, not new encoders.

Self-supervised learning (SSL). SSL strategies aim to learn representation from the input data itself, without relying on external labels. They can largely be categorized into contrastive or generative types. Contrastive SSL aims to maximize the agreement between data obtained from diverse views (Chen et al., 2020; Grill et al., 2020; You et al., 2020). Generative SSL, on the other hand, predicts or reconstructs parts of the input data. Success of generative SSL demonstrates its strengths in learning complex input data, in domains including natural language processing (Devlin et al., 2019; OpenAI, 2023) and computer vision (He et al., 2022; Tong et al., 2022). Recently, generative SSL for graphs has gained significant attention, with their main focuses on reconstructing edges (Tan et al., 2023; Li et al., 2023) or node features (Hou et al., 2022; 2023). ***Note***: Extending feature reconstruction from graphs to hypergraphs can be direct, which serves as our baseline method. However, it is non-trivial to extend the edge reconstruction methods for hyperedges (refer to Section 3.1).

Self-supervised learning on hypergraphs. The interest in SSL for hypergraphs is on the rise. Early hypergraph SSL strategies mainly targeted specific downstream tasks, such as group (Zhang et al., 2021) and session-based recommendation (Xia et al., 2022). Recent ones aim to obtain general-purpose representation. TriCL (Lee & Shin, 2023) utilizes a tri-directional contrastive loss, which consists of node-, hyperedge-, and membership-level contrast. Kim et al. (2023) enhances the scalability of TriCL with a partitioning technique. HyperGCL (Wei et al., 2022) generates views for contrast and empirically demonstrates its superiority over rule-based augmentation methods. ***Note***: (1) All the hypergraph SSL strategies are contrastive (rather than generative) and (2) no prior works establish a clear theoretical connection between their SSL strategies and downstream tasks.

3 PROPOSED TASK AND THEORETICAL ANALYSIS

In this section, after providing some preliminaries, we propose a novel generative SSL task on hypergraphs, *hyperedge filling*. Then, we establish a theoretical connection between hyperedge filling and node classification, which is a commonly-considered important downstream task.

Preliminaries. A hypergraph $\mathcal{G} = (\mathcal{V}, \mathcal{E})$ is defined by a node set $\mathcal{V}$ and a hyperedge set $\mathcal{E}$. Each hyperedge $e_j \in \mathcal{E}$ is a non-empty set of nodes (i.e., $\emptyset \neq e_j \subseteq \mathcal{V}, \forall e_j \in \mathcal{E}$). Each node $v_i \in \mathcal{V}$ is

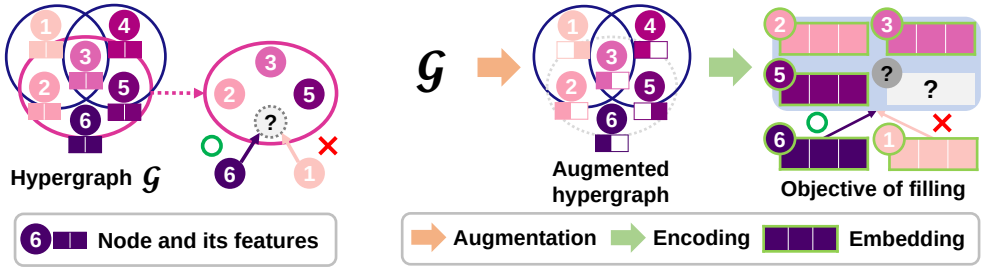

(a) Hyperedge filling task (b) Visual illustration of HYPEBOY

Figure 1: Overview of (a) the hyperedge filling task and (b) HYPEBOY, the proposed SSL method based on the task. The goal of the task is to find the missing node for a given query subset (i.e., the other nodes in a hyperedge). HYPEBOY trains HNNs aiming to correctly predict the missing node.

equipped with a feature vector $\boldsymbol{x}_i \in \mathbb{R}^d$, and $\mathbf{X} \in \mathbb{R}^{|\mathcal{V}| \times d}$ denotes the node feature matrix where the i-th row $\mathbf{X}_i$ corresponds to $\boldsymbol{x}_i$.

A hypergraph neural network (HNN) f_θ is a function that receives a node feature matrix $\mathbf{X}$ and a set of hyperedges $\mathcal{E}$ as inputs to return nodes embeddings $\mathbf{Z} \in \mathbb{R}^{|\mathcal{V}| \times k}$ (i.e., $\mathbf{Z} = f_\theta(\mathbf{X}, \mathcal{E})$, where θ is the set of learnable parameters).[1] ***Note***: Hypergraph self-supervised learning (SSL) aims to train f_θ by utilizing only $\mathbf{X}$ and $\mathcal{G}$, without any supervision from downstream task-related labels.

3.1 PROPOSED TASK: HYPEREDGE FILLING

We propose *hyperedge filling*, a generative SSL task for hypergraph representation learning. We first define the task and discuss the superiority of the proposed task over alternatives. An illustration of the hyperedge filling task is provided in Figure 1(a).

Task definition. Given a set of nodes, hyperedge filling aims to predict a node that is likely to form a hyperedge with it. Specifically, for each hyperedge $e_j \in \mathcal{E}$, we divide it into a (missing) node $v_i \in e_j$ and a (query) subset $q_{ij} = e_j \setminus \{v_i\}$. Then, the target of the task is to correctly fill the missing node v_i for each given subset q_{ij}. This can be formalized by maximizing the probability of v_i correctly completing q_{ij}, which is denoted as $p_{(\mathbf{X},\mathcal{E},\Theta)}(v_i \mid q_{ij})$, where Θ is a set of parameters we aim to optimize in this task. We will further elaborate on our design of $p_{(\mathbf{X},\mathcal{E},\Theta)}(\cdot)$ in Section 4.3.

Advantage over alternatives. Potential alternatives include naive extensions of generative SSL tasks for ordinary graphs: (a) generating hyperedges from scratch and (b) classifying given sets of nodes into real and fake hyperedges. Compared to (a), by shifting the focus of prediction from the set level (hyperedge itself) to the node level, the hyperedge filling task reduces the prediction space from computationally prohibitive $O(2^{|\mathcal{V}|})$ to affordable $O(|\mathcal{V}|)$. Compared to (b), the hyperedge filling task provides richer and more diversified generative SSL signals. Specifically, when considering a single hyperedge e_j, our task offers $|e_j|$ distinct node-subset combinations that can serve as SSL signals. In contrast, predicting the mere existence of e_j yields a singular and, thus, limited signal.

3.2 THEORETICAL RESULTS ON HYPEREDGE FILLING

To demonstrate the effect of hyperedge filling as a general SSL task, we present its theoretical connection to node classification. In essence, we demonstrate that node representations optimized for the hyperedge filling task can improve node classification accuracy. Then, we briefly discuss the theoretical difficulty of the task, showing that it has reasonable solutions for every hypergraph.

3.2.1 BASIC SETTING

First, we assume a data model of a hypergraph $\mathcal{G} = (\mathcal{V}, \mathcal{E})$, where (1) each node belongs to a single class, (2) the features of each node are generated from a Gaussian distribution, and (3) each hyper-

[1] In this paper, we assume HNNs return only vector representations of nodes unless otherwise stated, while we acknowledge that some HNNs return embeddings of hyperedges as well.

edge is generated according to a given homophilic ratio $\mathcal{P} \in [0.5, 1]$.[2] Specifically, if a hyperedge has a higher homophilic ratio $\mathcal{P}$, the hyperedge is more likely to contain nodes of the same class.

Assumption 1 (Node classes and features)**.** *Assume that there are $2N$ nodes and node classes C_1 and C_0 such that $C_1 \cup C_0 = \mathcal{V}, C_1 \cap C_0 = \emptyset$, and $|C_1| = |C_0| = N$. Each node feature vector $\boldsymbol{x}_i$ is independently generated from $\mathcal{N}(\boldsymbol{x}; \boldsymbol{\mu}_1, \boldsymbol{\Sigma})$ if $v_i \in C_1$, and $\mathcal{N}(\boldsymbol{x}; \boldsymbol{\mu}_0, \boldsymbol{\Sigma})$ if $v_i \in C_0$. For simplicity, we assume $\boldsymbol{\mu}_1 = (0.5)_{i=1}^d$, $\boldsymbol{\mu}_0 = (-0.5)_{i=1}^d$, and $\boldsymbol{\Sigma} = \mathbf{I}$, where $\mathbf{I}$ is the d-by-d identity matrix.*

Assumption 2 (Hypergraph topology)**.** *Assume that the number of hyperedges and the size of each hyperedge are given. There is no singleton hyperedge (i.e., $|e_j| \geq 2, \forall e_j \in \mathcal{E}$). Let B denote the binomial distribution. Each hyperedge $e_j \in \mathcal{E}$ has a membership $c_j \in \{0, 1\}$, where $c_j \sim B(1, 0.5)$. Given the number $|e_j|$ of nodes and the class $c_j \in \{0, 1\}$ of a hyperedge, the number of its members belonging to C_1 satisfies $|e_j \cap C_1| \sim B(|e_j|, \mathcal{P}^{c_j}(1-\mathcal{P})^{1-c_j})$.*

Second, we describe how node representations are updated via the hyperedge filling task. In this theoretical analysis, we define the updating process of node representations as follows:

(**F1**) Filling probability $p_{(\mathbf{X},\mathcal{E},\Theta)}(\cdot)$ is defined on each node-subset pair as follows:

$$p_{(\mathbf{X},\mathcal{E},\Theta)}(v_i \mid q_{ij}) := \frac{\exp(\boldsymbol{x}_i^T(\sum_{v_k \in q_{ij}} \boldsymbol{x}_k))}{\sum_{v_t \in \mathcal{V}} \exp(\boldsymbol{x}_t^T(\sum_{v_k \in q_{ij}} \boldsymbol{x}_k))}. \tag{1}$$

(**F2**) Node representation $\boldsymbol{z}_i$ is obtained via gradient descent with respect to $\boldsymbol{x}_i$ from $\mathcal{L}$, which is the negative log-likelihood of Eq. (1), (i.e., $\mathcal{L} = -\log p_{(\mathbf{X},\mathcal{E},\Theta)}(v_i \mid q_{ij})$). For ease of analysis, we assume $\boldsymbol{z}_i = \boldsymbol{x}_i - \gamma \nabla_{\boldsymbol{x}_i} \mathcal{L}$, where $\gamma \in \mathbb{R}^+$ is a fixed constant.

At last, we assume a Gaussian naive Bayes classifier $\mathcal{F}$ (Bishop, 2006), which is defined as:

$$\mathcal{F}(\boldsymbol{x}_i) = \underset{k \in \{0,1\}}{\arg\max}\, f(\boldsymbol{x}_i; \boldsymbol{\mu}_k, \mathbf{I}), \text{ where } f \text{ is the P.D.F. of } \mathcal{N}(\boldsymbol{x}; \boldsymbol{\mu}_k, \Sigma). \tag{2}$$

3.2.2 HYPEREDGE FILLING HELPS NODE CLASSIFICATION

Our goal is to show that for accurate classification of v_i, the representation $\boldsymbol{z}_i$, which is obtained for hyperedge filling as described in (**F1**) and (**F2**), is more effective than the original feature $\boldsymbol{x}_i$. First, we assume a node v_i belonging to the class C_1 (i.e., $v_i \in C_1$), and we later generalize the result to C_0. Then, the effectiveness of an original feature is defined as the expected accuracy of a classifier $\mathcal{F}$ with $\boldsymbol{x}_i$ (i.e., $\mathbb{E}_{\boldsymbol{x}}[\mathbf{1}_{\mathcal{F}(\boldsymbol{x}_i)=1}] := P_{\boldsymbol{x}}(f(\boldsymbol{x}_i; \boldsymbol{\mu}_1, \mathbf{I}) > f(\boldsymbol{x}_i; \boldsymbol{\mu}_0, \mathbf{I}))$). Similarly, that with a derived representation is defined as $\mathbb{E}_{\boldsymbol{z}}[\mathbf{1}_{\mathcal{F}(\boldsymbol{z}_i)=1}] = P_{\boldsymbol{z}}(f(\boldsymbol{z}_i; \boldsymbol{\mu}_1, \mathbf{I}) > f(\boldsymbol{z}_i; \boldsymbol{\mu}_0, \mathbf{I}))$. Below, we show that the effectiveness of a derived representation $\boldsymbol{z}_i$ is higher than that of an original feature $\boldsymbol{x}_i$.

Theorem 1 (Improvement in effectiveness)**.** *Assume a hyperedge e_j s.t. $e_j \cap C_1 \neq \emptyset$ and node features $\mathbf{X}$ that are generated under Assumption 1. For a node $v_i \in e_j \cap C_1$, the following holds:*

$$\boxed{\vec{\mathbf{1}}^T \sum_{v_k \in q_{ij}} \boldsymbol{x}_k > 0} \Rightarrow \mathbb{E}_{\boldsymbol{z}}[\mathbf{1}_{\mathcal{F}(\boldsymbol{z}_i)=1}] > \mathbb{E}_{\boldsymbol{x}}[\mathbf{1}_{\mathcal{F}(\boldsymbol{x}_i)=1}], \text{ where } \vec{\mathbf{1}} \text{ denotes } (1)_{k=1}^d. \tag{3}$$

Proof. Full proof is provided in Appendix A.1. □

Theorem 1 states that when a certain condition (boxed in Eq. (3)) is met, the effectiveness of $\boldsymbol{z}_i$ is greater than that of $\boldsymbol{x}_i$. This result implies that node representations, when refined using the objective function associated with the hyperedge filling task, are more proficient in performing accurate node classification compared to the original node features.

While the finding in Theorem 1 demonstrates the usefulness of the hyperedge filling task in node classification, its validity relies on the specific condition. We further analyze the probability that the condition is met by a stochastic G under Assumptions 1 and 2 for a given $\mathcal{P}$.

Theorem 2 (Realization of condition)**.** *Assume node features $\mathbf{X}$ and a hyperedge e_j s.t. (i) generated under Assumption 1 and 2 respectively, and (ii) $e_j \cap C_1 \neq \emptyset$. For any q_{ij} where $v_i \in C_1 \cap e_j$, the following holds:*

[2] We set $\mathcal{P} \in [0.5, 1]$ because generation process (Assumption 2) is symmetric about $\mathcal{P} = 0.5$ at $\mathcal{P} \in [0, 1]$ under binary class setting.

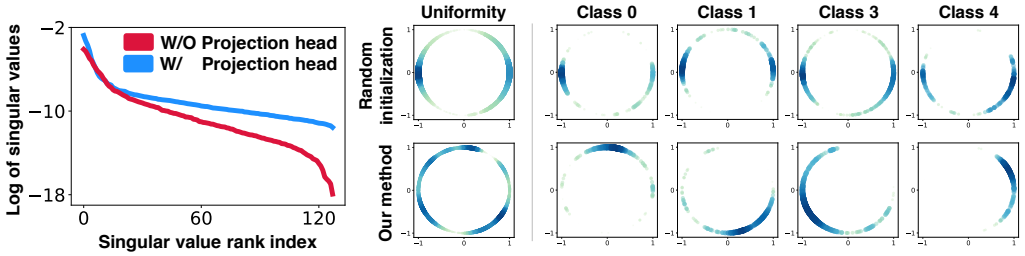

(a) Representation spectrum analysis. A sudden singular-value drop implies **dimensional collapse**.

(b) Representations on the unit hypersphere. Uniformly distributed representations achieve **uniformity**, and representations of nodes of the same class located close to each other achieve **alignment**.

Figure 2: Analysis regarding Property 2 (avoiding dimensional collapse) and Property 3 (representation uniformity and alignment) of HYPEBOY. As shown in (a), while HYPEBOY without projection heads (red) suffers from the dimensional collapse, HYPEBOY (blue) does not, demonstrating the necessity of the projection head. Furthermore, as shown in (b), representations from an HNN trained by HYPEBOY meet both uniformity and alignment, justifying our design choice of the loss function. Experiments are conducted on the Cora dataset.

1. $P_{\boldsymbol{x},e}\left(\mathbf{1}^T \sum_{v_k \in q_{ij}} \boldsymbol{x}_k > 0 \;\middle|\; \mathcal{P}\right) \geq 0.5, \forall \mathcal{P} \in [0.5, 1]$.
2. $P_{\boldsymbol{x},e}\left(\mathbf{1}^T \sum_{v_k \in q_{ij}} \boldsymbol{x}_k > 0 \;\middle|\; \mathcal{P}\right)$ *is a strictly increasing function w.r.t.* $\mathcal{P} \in [0.5, 1]$.

Proof. Full proof is provided in Appendix A.2. □

Theorem 2 states that the probability of the condition being satisfied is at least 0.5, if the homophilic ratio $\mathcal{P}$ is at least 0.5. Moreover, the likelihood of satisfying the condition strictly increases with respect to $\mathcal{P}$. Notably, many real-world group interactions exhibit homophilic traits (Laakasuo et al., 2020; Khanam et al., 2023). Therefore, the hyperedge filling task can improve node classification in many real-world scenarios, as evidenced by our theoretical findings and real-world characteristics.

Generalization to the class C_0. The above results can be easily generalized to the class C_0 due to the symmetry. Specifically, for each node $v_i \in C_0$, the effectiveness (spec., the expected accuracy of the classifier $\mathcal{F}$) of a derived representation $\boldsymbol{z}_i$ is greater than that of an original feature $\boldsymbol{x}_i$ under a certain condition. The probability of such a condition holding strictly increases from 0.5 with respect to the homophilic ratio $\mathcal{P} \in [0.5, 1]$. We theoretically show this in Appendices A.1 and A.2.

3.2.3 EXISTENCE OF REASONABLE SOLUTIONS

If a task is too difficult, it could be excessively challenging for a model to learn meaningful representations from the task. Fortunately, with a sufficiently large embedding dimension, our hyperedge filling task has "reasonable" solutions for every hypergraph, as shown theoretically in Appendix B.1.

4 PROPOSED METHOD FOR HYPEREDGE FILLING

In this section, we present **HYPEBOY** (**Hype**rgraphs, **b**uild **o**wn h**y**peredges), a hypergraph generative SSL method based on the proposed hyperedge filling task. HYPEBOY exhibits three desirable properties of hypergraph generative SSL, as empirically demonstrated later:

Property 1. Does not over-emphasize proximity information (Veličković et al., 2019).

Property 2. Avoids dimensional collapse (Jing et al., 2022) in node representations.

Property 3. Learns node representation to be aligned and uniform (Wang & Isola, 2020).

Our proposed method, HYPEBOY, is illustrated in Figure 1(b). After presenting each of its step, we discuss its **role** in satisfying the above properties. Lastly, we introduce a novel two-stage training scheme for further enhancing HYPEBOY.

4.1 STEP 1: HYPERGRAPH AUGMENTATION

HYPEBOY first obtains augmented feature matrix $\mathbf{X}'$ and hyperedge set $\mathcal{E}'$ by using augmentation functions $\boldsymbol{\tau}_{\boldsymbol{x}}$ and $\boldsymbol{\tau}_{\mathcal{E}}$, respectively. The feature augmentation function $\boldsymbol{\tau}_{\boldsymbol{x}} : (\mathbf{X}, p_v) \mapsto \mathbf{X}'$ masks certain entries of $\mathbf{X}$ based on Bernoulli sampling (spec., $\mathbf{X}' = \mathbf{X} \odot \mathbf{M}$, where $\odot$ is an element-wise product and $\mathbf{M}_{ij} \sim B(1, p_v), \forall i \in [|\mathcal{V}|], j \in [d]$). The topology augmentation function $\boldsymbol{\tau}_{\mathcal{E}} : (\mathcal{E}, p_e) \mapsto \mathcal{E}'$ samples $\lceil |\mathcal{E}|(1-p_e) \rceil$ hyperedges uniformly at random from $\mathcal{E}$. Note that the magnitudes of feature and topology augmentations are proportional to $p_v, p_e \in [0, 1]$, respectively.

Role. For hypergraph SSL, augmentations are crucial for mitigating overly-emphasized proximity information. That is, using all hyperedges and/or features for both message passing and objective-function construction may risk HNNs to heavily rely on direct neighborhood information (Tan et al., 2023). Many graph SSL strategies mask certain input edges and/or node features, allowing their encoder models to not overfit to the neighbor distribution and features (Hou et al., 2022; Li et al., 2023; Tan et al., 2023). Motivated by their findings, we employ the augmentation step. In Appendix E.1, we demonstrate that augmentation enhances node classification performance of HYPEBOY.

4.2 STEP 2: HYPERGRAPH ENCODING

After augmentation, HYPEBOY obtains node and query subset representations. First, HYPEBOY obtains node embeddings $\mathbf{Z} \in \mathbb{R}^{|\mathcal{V}| \times d'}$ by feeding the augmented hypergraph into an encoder HNN: $\mathbf{Z} = f_\theta(\mathbf{X}', \mathcal{E}')$. Then, HYPEBOY obtains projected representations of query subsets (i.e., $q_{ij}, v_i \in e_j, e_j \in \mathcal{E}$) and nodes. To this end, we utilize a node projection head f'_ϕ and a set projection head f''_ψ. Specifically, projected embeddings of node v_i and query subset q_{ij} are $\boldsymbol{h}_i = f'_\phi(\boldsymbol{z}_i) \in \mathbb{R}^k$ and $\boldsymbol{q}_{ij} = f''_\rho(\sum_{v_t \in q_{ij}} \boldsymbol{z}_t) \in \mathbb{R}^k$, respectively. Here, the design choice of a set projection head is motivated by Deep Sets (Zaheer et al., 2017).

Role. We investigate the role of the projection heads, which are non-trivial components, in the context of the dimensional collapse of embeddings. Dimensional collapse is a phenomenon in which embedding vectors occupy only the lower dimensional sub-space of their full dimension (Jing et al., 2022). This is identified by observing whether or not certain singular values of the embedding covariance matrix drop to zero. To prevent dimensional collapse, we employ projection heads in HYPEBOY, and this is in line with the prior findings of Jing et al. (2022) and Song et al. (2023). Figure 2(a) illustrates that an HNN trained using HYPEBOY avoids dimensional collapse, whereas an HNN trained with its variant (without projection heads) does not. Results on more datasets are in Appendix E.2. Furthermore, we provide a theoretical analysis on why HYPEBOY without projection heads may suffer from dimensional collapse in Appendix B.2. Note that this distinction leads to a performance discrepancy in node classification (Section 5.3).

4.3 STEP 3: HYPEREDGE FILLING LOSS

The last step is to compute the SSL loss based on the hyperedge filling probability. We design $p_{(\mathbf{X},\mathcal{E},\Theta)}(v_k \mid q_{ij})$ to be normalized over $\mathcal{V}$ (i.e., $\sum_{v_k \in \mathcal{V}} p_{(\mathbf{X},\mathcal{E},\Theta)}(v_k \mid q_{ij}) = 1$). To this end, we utilize a Softmax to model probabilities. In sum, with projected embeddings $\boldsymbol{h}_i$ and $\boldsymbol{q}_{ij}$ (Section 4.2), the probability of a node v_i completing a query subset q_{ij} is defined as follows:

$$p_{(\mathbf{X},\mathcal{E},\Theta)}(v_i \mid q_{ij}) := \frac{\exp(sim(\boldsymbol{h}_i, \boldsymbol{q}_{ij}))}{\sum_{v_k \in \mathcal{V}} \exp(sim(\boldsymbol{h}_k, \boldsymbol{q}_{ij}))}, \tag{4}$$

where sim is the cosine similarity function (other similarity functions are also applicable). Here, HYPEBOY optimizes for all possible hyperedge filling cases (i.e., $\Pi_{e_j \in \mathcal{E}} \Pi_{v_i \in e_j} p_{(\mathbf{X},\mathcal{E},\Theta)}(v_i \mid q_{ij})$). Lastly, HYPEBOY minimizes the negative log-likelihood of all possible cases as follows:

$$\mathcal{L} := -\sum_{e_j \in \mathcal{E}} \sum_{v_i \in e_j} \log \frac{\exp(sim(\boldsymbol{h}_i, \boldsymbol{q}_{ij}))}{\sum_{v_k \in \mathcal{V}} \exp(sim(\boldsymbol{h}_k, \boldsymbol{q}_{ij}))}. \tag{5}$$

Note that the set Θ of all parameters consists of the parameters of the encoder HNN f_θ, the node projection head f'_ϕ, and the set projection head f''_ρ (i.e., $\Theta = (\theta, \phi, \rho)$). They are updated by gradient descent, aiming to minimize the loss $\mathcal{L}$ defined in Eq. (5).

Role. Our design choice of $p_{(\mathbf{X},\mathcal{E},\Theta)}(\cdot)$ ensures that representations learned via HYPEBOY achieve both alignment and uniformity (Wang & Isola, 2020). In our case, *alignment* indicates that node embeddings belonging to the same class are closely located to each other, and *uniformity* indicates that embeddings are uniformly distributed over the embedding space. Through the numerator of Eq. (5), HYPEBOY pulls representations of a missing node and a query subset, promoting the alignment as discussed in our theoretical analysis (Section 3.2). At the same time, the denominator of Eq. (5) pushes away every node representation from each query subset representation, encouraging that representations are uniformly distributed. This intuition is supported by the findings of Wang & Isola (2020): the denominators of their contrastive loss, which push away representations from each other, encourage uniformity. As shown in Figure 2(b), we verify that node representations from HYPEBOY achieve both alignment and uniformity. Results on more datasets are in Appendix E.3.

4.4 TWO-STAGE TRAINING SCHEME FOR FURTHER ENHANCEMENT

We propose a novel two-stage training scheme to further enhance the effectiveness of HYPEBOY.

Challenges: heavy reliance on projection heads. In our preliminary studies, we observed that during training, HYPEBOY often relies heavily on projection heads rather than the parameters of encoder HNNs. Consequently, HNNs are pre-trained suboptimally.

Solution: warming-up encoders via feature reconstruction. To reduce this reliance on projection heads, we introduce a *warm-up* training stage. Firstly, we train the parameters (i.e., the parameter of an encoder HNN and projection heads), aiming for node-feature reconstruction, where projection heads play a less prominent role. Then, the parameters of the encoder HNN (excluding the projection heads) are employed to initialize the HNN encoder of HYPEBOY. This initialization strengthens the HNN encoders, thereby reducing the reliance on projection heads. For details and effectiveness of this warm-up stage, refer to Appendix D.3 and Section 5.3, respectively.

5 EXPERIMENTAL RESULTS

We now evaluate the efficacy of HYPEBOY as techniques for (1) pre-training hypergraph neural networks (HNNs) for node classification (Section 5.1) and (2) learning general-purpose representations (Section 5.2). Then, we justify each of its component through an ablation study (Section 5.3).

Datasets. For experiments, we use 11 benchmark hypergraph datasets. The hypergraph datasets are from diverse domains, expressing co-citation, co-authorship, computer graphics, movie-actor, news, and political membership relations. In Appendix C, we detail their statistics and descriptions.

Baselines methods. We utilize 15 baseline methods. They include (a) 10 *(semi-)supervised HNNs*, including ED-HNN (Wang et al., 2023a) and PhenomNN (Wang et al., 2023b), (b) 2 latest *generative SSL* strategies for ordinary graphs (GraphMAE2 (Hou et al., 2023) and MaskGAE (Liu et al., 2022)), and (3) 3 *contrastive SSL* strategies for hypergraph (TriCL (Lee & Shin, 2023), HyperGCL (Wei et al., 2022), and H-GD, which is a direct extension of a graph SSL method (Zheng et al., 2022) to hypergraphs). We use UniGCNII (Huang & Yang, 2021) and GCN (Kipf & Welling, 2017) as the encoders for hypergraph SSL methods and graph SSL methods, respectively.[3] In Appendix D, we provide their details, including their implementations, training, and hyperparameters.

HYPEBOY. We employ UniGCNII as an encoder of HYPEBOY, which is the same as that of other hypergraph SSL methods. For both node- and set projection heads, we use an MLP. Further details of HYPEBOY, including its implementations and hyperparameters, are provided in Appendix D.3.

5.1 EFFICACY AS A PRE-TRAINING TECHNIQUE (FINE-TUNED EVALUATION)

Setup. Following Wei et al. (2022), we randomly split the nodes into training/validation/test sets with the ratio of 1%/1%/98%, respectively.[4] For reliability, we assess each method on 20 data splits across 5 random initializations, as suggested in (Lee & Shin, 2023). We report the average (AVG) and standard deviation (STD) of test accuracy values on each dataset. Specifically, for each

[3]We choose the encoders that achieve the best overall performances. In our preliminary study, we find that UniGCNII and GCN generally work best and even outperform the encoders used in the original works.

[4]We ensure that a training set includes at least one node from each class.

Table 1: Efficacy as pre-training techniques: AVG and STD of accuracy values in node classification under the **fine-tuning protocol.** The best and second-best performances are colored green and yellow, respectively. R.G. and A.R. denote the random guess and average ranking among all methods, respectively. O.O.T. means that training is not completed within 24 hours. HYPEBOY outperforms all the baseline methods in 8 datasets, and overall, it obtains the best average ranking.

	Method	Citeseer	Cora	Pubmed	Cora-CA	DBLP-P	DBLP-A	AMiner	IMDB	MN-40	20News	House	A.R.
(Semi-)Supervised	R.G.	18.1 (0.9)	17.4 (1.0)	36.0 (0.7)	17.8 (0.7)	18.9 (0.2)	25.6 (1.0)	10.2 (0.2)	33.9 (0.7)	3.7 (0.2)	50.1 (1.3)	26.7 (0.3)	16.9
	MLP	32.5 (7.0)	27.9 (7.0)	62.1 (3.7)	34.8 (5.1)	73.5 (1.0)	56.0 (4.9)	22.3 (1.7)	39.1 (2.4)	89.4 (1.5)	73.1 (1.4)	72.2 (3.9)	13.4
	HGNN	41.9 (7.8)	50.0 (7.2)	72.9 (5.0)	50.2 (5.7)	85.3 (0.8)	67.1 (6.0)	30.3 (2.5)	42.2 (2.9)	88.0 (1.4)	76.4 (1.9)	52.7 (3.8)	10.0
	HyperGCN	31.4 (9.5)	33.1 (10.2)	63.5 (14.4)	37.1 (9.1)	53.5 (11.6)	68.2 (14.4)	26.4 (3.6)	37.9 (4.5)	55.1 (7.8)	67.0 (9.4)	49.8 (3.5)	14.7
	HNHN	43.1 (8.7)	50.0 (7.9)	72.1 (5.4)	48.3 (6.2)	84.6 (0.9)	62.6 (4.8)	30.0 (2.4)	42.3 (3.4)	86.1 (1.6)	74.2 (1.5)	49.7 (2.2)	11.9
	UniGCN	44.2 (8.1)	49.1 (8.4)	74.4 (3.9)	51.3 (6.3)	86.9 (0.6)	65.1 (4.7)	32.7 (1.8)	41.6 (3.5)	89.1 (1.0)	77.2 (1.2)	51.1 (2.4)	9.1
	UniGIN	40.4 (9.1)	47.8 (7.7)	69.8 (5.6)	48.3 (6.1)	83.4 (0.8)	63.4 (5.1)	30.2 (1.4)	41.4 (2.7)	88.2 (1.8)	70.6 (1.8)	51.1 (3.0)	13.0
	UniGCNII	44.2 (9.0)	48.5 (7.4)	74.1 (3.9)	54.8 (7.5)	87.4 (0.6)	65.8 (3.9)	32.5 (1.7)	42.5 (3.9)	90.8 (1.1)	70.9 (1.0)	50.8 (4.3)	8.8
	AllSet	43.5 (8.0)	47.6 (4.2)	72.4 (4.5)	57.5 (5.7)	85.9 (0.6)	65.3 (3.9)	29.3 (1.2)	42.3 (2.4)	92.1 (0.6)	71.9 (2.5)	54.1 (3.4)	9.8
	ED-HNN	40.3 (8.0)	47.6 (7.7)	72.7 (4.7)	54.8 (5.4)	86.2 (0.8)	65.8 (4.8)	30.0 (2.1)	41.4 (3.0)	90.7 (0.9)	76.2 (1.2)	71.3 (3.7)	9.6
	PhenomNN	49.8 (9.6)	56.4 (9.6)	76.1 (3.5)	60.8 (6.2)	88.1 (0.4)	72.3 (4.1)	33.8 (2.0)	44.1 (3.7)	95.9 (0.8)	74.0 (1.5)	70.4 (5.6)	3.9
Self-supervised	GraphMAE2	41.1 (10.0)	49.3 (8.3)	72.9 (4.2)	55.4 (8.4)	86.6 (0.6)	69.5 (4.4)	32.8 (1.9)	43.3 (2.7)	90.1 (0.7)	71.9 (1.3)	52.8 (3.5)	8.4
	MaskGAE	49.6 (10.1)	57.1 (8.8)	72.8 (4.3)	57.8 (5.9)	86.3 (0.5)	74.8 (3.1)	33.7 (1.6)	44.5 (2.5)	90.0 (0.9)	O.O.T.	51.8 (3.3)	7.4
	TriCL	51.7 (9.8)	60.2 (7.9)	76.2 (3.6)	64.3 (5.5)	88.0 (0.4)	79.7 (2.9)	33.1 (2.2)	46.9 (2.9)	90.3 (1.0)	77.2 (1.0)	69.7 (4.9)	3.4
	HyperGCL	47.0 (9.2)	60.3 (7.4)	76.8 (3.7)	62.0 (5.1)	87.6 (0.5)	79.7 (3.8)	33.2 (1.6)	43.9 (3.6)	91.2 (0.8)	77.8 (0.8)	69.2 (4.9)	3.5
	H-GD	45.4 (9.9)	50.6 (8.2)	74.5 (3.5)	58.8 (6.2)	87.3 (0.5)	75.1 (3.6)	32.6 (2.2)	43.0 (3.3)	90.0 (1.0)	77.2 (1.0)	69.7 (5.1)	5.8
	HYPEBOY	56.7 (9.8)	62.3 (7.7)	77.0 (3.4)	66.3 (4.6)	88.2 (0.4)	80.6 (2.3)	34.1 (2.2)	47.6 (2.5)	90.4 (0.9)	77.6 (0.9)	70.4 (4.8)	1.7

SSL strategy, including HYPEBOY, we pre-train a backbone encoder with the corresponding SSL scheme and then fine-tune the encoder in a (semi-)supervised manner.

Results. As shown in Table 1, HYPEBOY shows the best average ranking among all 17 methods. Two points stand out. First, pre-training an HNN with HYPEBOY generally improves node classification. Compared to the performance of UniGCNII (HYPEBOY's backbone encoder), HYPEBOY obtains performance gains up to 12.5 points in 10 out of 11 datasets. Second, HYPEBOY outperforms all other SSL strategies. Specifically, compared to the second-best method (TriCL) the accuracy gap is up to 5.0 points. In addition, the suboptimal performance of the SOTA generative SSL strategies for graphs (i.e. GraphMAE2 and MaskGAE) implies the importance of preserving higher-order interactions in learning hypergraph representations.[5] In summary, HYPEBOY serves as an effective SSL strategy to pre-train HNNs for node classification.

5.2 EFFICACY AS A GENERAL-PURPOSE EMBEDDING TECHNIQUE (LINEAR EVALUATION)

Setup. We assess the generalizability of learned representations from HYPEBOY in two downstream tasks: node classification and hyperedge prediction. Considering this objective, we limit the baseline methods to SSL strategies, which yield embeddings independent of downstream tasks, and the original node features (i.e., naive $\mathbf{X}$). We use the linear evaluation protocol, i.e., the embeddings are used as **fixed** inputs to the classifiers for each task. For node classification, we use the same settings described in Section 5.1. For hyperedge prediction, we split hyperedges into training/validation/test sets by the ratio of 60%/20%/20%. For its evaluation, we obtain the same number of negative hyperedge samples as that of the ground-truth hyperedges (Patil et al., 2020). We report the average (AVG) and standard deviation (STD) of test AUROC values on each dataset. Further experimental details about hyperedge prediction, including negative sampling, are provided in Appendix D.3.

Results. As shown in Table 2, HYPEBOY has the best average ranking in both node classification and hyperedge prediction. Specifically, in node classification, compared to the second-best method (TriCL), the accuracy gap is up to 6.3 points. This demonstrates that HYPEBOY is more effective in learning general-purpose hypergraph representations than the other SSL strategies on hypergraphs.

5.3 ABLATION STUDY

We analyze the necessity for each component of HYPEBOY, specifically, (a) the hyperedge filling task (Section 3.1), (b) projection heads (Section 4.2), and (c) the feature reconstruction warm-up

[5] Representing higher-order interactions with a graph can cause the information loss (Dong et al., 2020).

Table 2: Efficacy as general-purpose embedding techniques: AVG and STD of accuracy/AUROC values in node-classification/hyperedge-prediction under the **linear evaluation protocol**. In each downstream task, the best and second-best performances are colored green and yellow, respectively. A.R. denotes the average ranking among all methods. O.O.T. means that training is not completed within 24 hours. HYPEBOY obtains the best average ranking in both downstream tasks.

	Method	Citeseer	Cora	Pubmed	Cora-CA	DBLP-P	DBLP-A	AMiner	IMDB	MN-40	20News	House	A.R.
Node classification	Naive **X**	27.8 (7.0)	32.4 (4.6)	62.8 (2.8)	31.9 (5.5)	69.4 (0.7)	54.7 (4.7)	21.4 (1.2)	38.1 (1.9)	91.9 (1.1)	70.6 (1.9)	71.3 (5.4)	5.0
	GraphMAE2	29.2 (6.5)	37.5 (7.0)	55.5 (9.5)	38.2 (9.1)	75.6 (1.7)	57.5 (5.6)	27.3 (2.7)	36.6 (3.5)	89.1 (1.8)	62.3 (2.3)	51.7 (3.5)	5.6
	MaskGAE	47.2 (11.1)	56.8 (9.3)	62.6 (5.5)	56.0 (4.8)	84.8 (0.7)	75.1 (3.5)	33.2 (2.0)	44.1 (3.9)	90.5 (0.9)	O.O.T.	50.0 (2.8)	4.4
	TriCL	53.3 (10.0)	62.1 (8.8)	74.5 (4.1)	63.6 (5.2)	87.1 (0.7)	80.9 (3.2)	35.0 (3.6)	48.0 (3.2)	80.0 (5.1)	67.2 (4.0)	69.1 (5.5)	2.5
	HyperGCL	42.6 (8.6)	61.8 (8.3)	67.6 (8.0)	58.1 (6.3)	56.6 (5.2)	79.8 (3.8)	33.3 (2.2)	47.5 (2.8)	84.1 (2.8)	71.2 (3.4)	67.1 (5.4)	3.8
	H-GD	35.6 (7.8)	37.6 (6.8)	58.0 (8.2)	48.6 (7.4)	73.3 (1.3)	74.0 (3.3)	33.8 (5.0)	35.2 (2.9)	76.6 (4.4)	54.8 (7.4)	68.3 (5.7)	5.3
	HYPEBOY	59.6 (9.9)	63.5 (9.4)	75.0 (3.4)	66.0 (4.6)	87.9 (0.5)	81.2 (2.7)	34.3 (3.2)	48.8 (1.8)	89.2 (2.2)	75.7 (2.1)	69.4 (5.4)	1.4
Hyperedge prediction	Naive **X**	63.3 (2.1)	75.5 (1.6)	88.3 (0.6)	55.0 (1.9)	90.0 (0.4)	72.1 (1.3)	80.0 (1.1)	39.5 (1.9)	99.5 (0.1)	97.7 (2.9)	54.8 (5.0)	5.8
	GraphMAE2	73.3 (2.7)	76.4 (1.7)	81.6 (1.1)	76.3 (3.1)	85.2 (0.4)	68.3 (1.8)	80.7 (0.9)	53.7 (2.6)	99.5 (0.1)	90.1 (5.7)	62.9 (3.8)	5.5
	MaskGAE	86.1 (1.6)	88.5 (1.4)	92.9 (0.5)	81.8 (2.7)	93.2 (0.5)	79.3 (2.0)	84.6 (0.1)	58.1 (2.5)	99.3 (0.1)	O.O.T.	87.0 (3.4)	4.0
	TriCL	90.5 (1.2)	90.7 (1.3)	91.9 (0.5)	87.8 (1.5)	94.8 (0.2)	87.9 (1.4)	90.4 (0.6)	58.9 (2.1)	99.6 (0.1)	98.2 (3.0)	90.0 (2.6)	1.8
	HyperGCL	73.9 (2.6)	85.4 (1.5)	89.6 (0.5)	81.1 (1.9)	83.6 (0.6)	83.5 (1.0)	82.1 (7.6)	53.8 (2.4)	99.4 (0.1)	96.7 (7.0)	76.3 (6.3)	4.5
	H-GD	72.2 (5.0)	71.9 (3.1)	87.2 (0.7)	73.2 (4.0)	91.6 (1.0)	81.4 (1.9)	84.9 (2.1)	53.1 (1.8)	99.5 (0.1)	83.9 (2.1)	87.9 (3.1)	4.9
	HYPEBOY	91.1 (1.1)	91.9 (1.1)	95.1 (0.3)	88.1 (1.4)	95.5 (0.1)	87.3 (1.3)	89.8 (0.5)	59.4 (2.1)	99.7 (0.1)	99.0 (1.6)	87.0 (2.8)	1.4

Table 3: The ablation study with four variants of HYPEBOY on node classification under the fine-tuning protocol. The best and second-best performances are colored green and yellow, respectively. F.R., H.F., and P.H. denote Feature Reconstruction, Hyperedge Filling, and Projection Heads, respectively. A.R. denotes the average ranking among all methods. HYPEBOY outperforms others in most datasets, justifying each of its components.

	F. R.	H. F.	P. H.	Citeseer	Cora	Pubmed	Cora-CA	DBLP-P	DBLP-A	AMiner	IMDB	MN-40	20News	House	A.R.
V1	✗	✔	✗	51.6 (11.2)	60.7 (8.2)	76.2 (3.6)	63.5 (0.6)	88.1 (0.5)	78.5 (2.9)	33.5 (2.8)	46.8 (3.1)	90.0 (1.1)	77.4 (0.9)	68.5 (4.5)	4.1
V2	✗	✔	✔	52.7 (9.6)	59.7 (9.2)	76.7 (3.2)	63.5 (0.6)	88.2 (0.5)	79.1 (2.5)	33.8 (2.2)	46.9 (3.3)	90.6 (1.0)	77.0 (0.9)	69.6 (4.9)	3.2
V3	✔	✗	✗	52.0 (9.3)	58.9 (8.2)	74.1 (3.9)	61.2 (6.6)	87.8 (0.4)	79.9 (2.3)	33.9 (2.1)	46.3 (2.7)	91.4 (0.9)	77.5 (0.9)	70.1 (4.8)	3.6
V4	✔	✔	✗	56.0 (9.9)	61.8 (8.5)	76.5 (3.1)	65.3 (4.3)	88.0 (0.4)	80.3 (2.4)	34.0 (2.0)	47.5 (2.3)	90.8 (1.0)	77.4 (1.0)	69.3 (5.0)	2.5
Ours	✔	✔	✔	56.7 (9.8)	62.3 (7.7)	77.0 (3.4)	66.3 (4.6)	88.2 (0.4)	80.6 (2.3)	34.1 (2.2)	47.6 (2.5)	90.4 (0.9)	77.6 (0.9)	70.4 (4.8)	1.3

(Section 4.4). To this end, we utilize four variants of HYPEBOY: **(V1)**: without feature reconstruction warm-up and projection heads, **(V2)**: without feature reconstruction warm-up[6], **(V3)**: without the hyperedge filling process, and **(V4)**: without projection heads. Here, projection heads are used only for methods with the hyperedge filling process. Note that **(V3)** is a direct extension of feature reconstructing SSL methods for graphs to hypergraphs.

As shown in Table 3, HYPEBOY, equipped with all of its components, outperforms the others in most datasets, demonstrating the effectiveness of our design choices. There are two other notable results. First, the necessity of projection heads is evidenced by the superior performance of **V2** (compared to **V1**) and ours (compared to **V4**). Second, the advantage of the hyperedge filling task over feature reconstruction is manifested by the better average rank of **V2** compared to **V3**.

6 CONCLUSION

In this work, we conduct a comprehensive analysis of generative self-supervised learning on hypergraphs. Our contribution is three-fold. First, we propose the hyperedge filling task, a generative self-supervised learning task on hypergraphs, and investigate the theoretical connection between the task and node classification (Section 3). Second, we present a generative SSL method HYPEBOY to solve the proposed task (Section 4). Third, we demonstrate the superiority of HYPEBOY over existing SSL methods on hypergraphs through extensive experiments (Section 5). Code and datasets are available at `link`.

[6]In order to mitigate an issue of over-relying on projection heads (Section 4.4), we have trained an encoder without projection heads at the beginning, and after some epochs, we train the encoder with projection heads.

REFERENCES

Christopher M. Bishop. *Pattern Recognition and Machine Learning*. Springer, 2006.

Ting Chen, Simon Kornblith, Mohammad Norouzi, and Geoffrey Hinton. A simple framework for contrastive learning of visual representations. In *ICML*, 2020.

Eli Chien, Chao Pan, Jianhao Peng, and Olgica Milenkovic. You are allset: A multiset function framework for hypergraph neural networks. In *ICLR*, 2022.

Jacob Devlin, Ming-Wei Chang, Kenton Lee, and Kristina Toutanova. Bert: Pre-training of deep bidirectional transformers for language understanding. In *NACCL*, 2019.

Yihe Dong, Will Sawin, and Yoshua Bengio. Hnhn: Hypergraph networks with hyperedge neurons. In *ICML Workshop on Graph Representation Learning and Beyond (GRL+)*, 2020.

Dheeru Dua, Casey Graff, et al. Uci machine learning repository. 2017.

Yifan Feng, Zizhao Zhang, Xibin Zhao, Rongrong Ji, and Yue Gao. Gvcnn: Group-view convolutional neural networks for 3d shape recognition. In *CVPR*, 2018.

Yifan Feng, Haoxuan You, Zizhao Zhang, Rongrong Ji, and Yue Gao. Hypergraph neural networks. In *AAAI*, 2019.

Jean-Bastien Grill, Florian Strub, Florent Altché, Corentin Tallec, Pierre Richemond, Elena Buchatskaya, Carl Doersch, Bernardo Avila Pires, Zhaohan Guo, Mohammad Gheshlaghi Azar, et al. Bootstrap your own latent-a new approach to self-supervised learning. In *NeurIPS*, 2020.

Kaiming He, Xinlei Chen, Saining Xie, Yanghao Li, Piotr Dollár, and Ross Girshick. Masked autoencoders are scalable vision learners. In *CVPR*, 2022.

Zhenyu Hou, Xiao Liu, Yukuo Cen, Yuxiao Dong, Hongxia Yang, Chunjie Wang, and Jie Tang. Graphmae: Self-supervised masked graph autoencoders. In *KDD*, 2022.

Zhenyu Hou, Yufei He, Yukuo Cen, Xiao Liu, Yuxiao Dong, Evgeny Kharlamov, and Jie Tang. Graphmae2: A decoding-enhanced masked self-supervised graph learner. In *WWW*, 2023.

Jing Huang and Jie Yang. Unignn: a unified framework for graph and hypergraph neural networks. In *IJCAI*, 2021.

Li Jing, Pascal Vincent, Yann LeCun, and Yuandong Tian. Understanding dimensional collapse in contrastive self-supervised learning. In *ICLR*, 2022.

Kazi Zainab Khanam, Gautam Srivastava, and Vijay Mago. The homophily principle in social network analysis: A survey. *Multimedia Tools and Applications*, 82(6):8811–8854, 2023.

Sunwoo Kim, Dongjin Lee, Yul Kim, Jungho Park, Taeho Hwang, and Kijung Shin. Datasets, tasks, and training methods for large-scale hypergraph learning. *Data Mining and Knowledge Discovery*, pp. 1–39, 2023.

Diederik P Kingma and Jimmy Ba. Adam: A method for stochastic optimization. In *ICLR*, 2015.

Thomas N Kipf and Max Welling. Semi-supervised classification with graph convolutional networks. In *ICLR*, 2017.

Michael Laakasuo, Anna Rotkirch, Max Van Duijn, Venla Berg, Markus Jokela, Tamas David-Barrett, Anneli Miettinen, Eiluned Pearce, and Robin Dunbar. Homophily in personality enhances group success among real-life friends. *Frontiers in Psychology*, 11:710, 2020.

Dongjin Lee and Kijung Shin. I'm me, we're us, and i'm us: Tri-directional contrastive learning on hypergraphs. In *AAAI*, 2023.

Jintang Li, Ruofan Wu, Wangbin Sun, Liang Chen, Sheng Tian, Liang Zhu, Changhua Meng, Zibin Zheng, and Weiqiang Wang. What's behind the mask: Understanding masked graph modeling for graph autoencoders. In *KDD*, 2023.

Xuan Liu, Congzhi Song, Shichao Liu, Menglu Li, Xionghui Zhou, and Wen Zhang. Multi-way relation-enhanced hypergraph representation learning for anti-cancer drug synergy prediction. *Bioinformatics*, 38(20):4782–4789, 2022.

Vinod Nair and Geoffrey E Hinton. Rectified linear units improve restricted boltzmann machines. In *ICML*, 2010.

OpenAI. Gpt-4 technical report. 2023.

Prasanna Patil, Govind Sharma, and M Narasimha Murty. Negative sampling for hyperlink prediction in networks. In *PAKDD*, 2020.

Ding Ruan, Shuyi Ji, Chenggang Yan, Junjie Zhu, Xibin Zhao, Yuedong Yang, Yue Gao, Changqing Zou, and Qionghai Dai. Exploring complex and heterogeneous correlations on hypergraph for the prediction of drug-target interactions. *Patterns*, 2(12), 2021.

Khaled Mohammed Saifuddin, Briana Bumgardner, Farhan Tanvir, and Esra Akbas. Hygnn: Drug-drug interaction prediction via hypergraph neural network. In *ICDE*, 2023.

Ramit Sawhney, Shivam Agarwal, Arnav Wadhwa, and Rajiv Ratn Shah. Spatiotemporal hypergraph convolution network for stock movement forecasting. In *ICDM*, 2020.

Ramit Sawhney, Shivam Agarwal, Arnav Wadhwa, Tyler Derr, and Rajiv Ratn Shah. Stock selection via spatiotemporal hypergraph attention network: A learning to rank approach. In *AAAI*, 2021.

Zeen Song, Xingzhe Su, Jingyao Wang, Wenwen Qiang, Changwen Zheng, and Fuchun Sun. Towards the sparseness of projection head in self-supervised learning. *arXiv preprint arXiv:2307.08913*, 2023.

Hang Su, Subhransu Maji, Evangelos Kalogerakis, and Erik Learned-Miller. Multi-view convolutional neural networks for 3d shape recognition. In *CVPR*, 2015.

Qiaoyu Tan, Ninghao Liu, Xiao Huang, Soo-Hyun Choi, Li Li, Rui Chen, and Xia Hu. S2gae: Self-supervised graph autoencoders are generalizable learners with graph masking. In *WSDM*, 2023.

`link`. Code and datasets are available at here. URL `https://anonymous.4open.science/r/hypeboy-1B00`.

Zhan Tong, Yibing Song, Jue Wang, and Limin Wang. Videomae: Masked autoencoders are data-efficient learners for self-supervised video pre-training. 2022.

Petar Veličković, William Fedus, William L Hamilton, Pietro Liò, Yoshua Bengio, and R Devon Hjelm. Deep graph infomax. In *ICLR*, 2019.

Peihao Wang, Shenghao Yang, Yunyu Liu, Zhangyang Wang, and Pan Li. Equivariant hypergraph diffusion neural operators. In *ICLR*, 2023a.

Tongzhou Wang and Phillip Isola. Understanding contrastive representation learning through alignment and uniformity on the hypersphere. In *ICML*, 2020.

Xiao Wang, Houye Ji, Chuan Shi, Bai Wang, Yanfang Ye, Peng Cui, and Philip S Yu. Heterogeneous graph attention network. In *WWW*, 2019.

Yuxin Wang, Quan Gan, Xipeng Qiu, Xuanjing Huang, and David Wipf. From hypergraph energy functions to hypergraph neural networks. In *ICML*, 2023b.

Tianxin Wei, Yuning You, Tianlong Chen, Yang Shen, Jingrui He, and Zhangyang Wang. Augmentations in hypergraph contrastive learning: Fabricated and generative. In *NeurIPS*, 2022.

Zhirong Wu, Shuran Song, Aditya Khosla, Fisher Yu, Linguang Zhang, Xiaoou Tang, and Jianxiong Xiao. 3d shapenets: A deep representation for volumetric shapes. In *CVPR*, 2015.

Lianghao Xia, Chao Huang, and Chuxu Zhang. Self-supervised hypergraph transformer for recommender systems. In *KDD*, 2022.

Naganand Yadati, Madhav Nimishakavi, Prateek Yadav, Vikram Nitin, Anand Louis, and Partha Talukdar. Hypergcn: A new method for training graph convolutional networks on hypergraphs. In *NeurIPS*, 2019.

Yuning You, Tianlong Chen, Yongduo Sui, Ting Chen, Zhangyang Wang, and Yang Shen. Graph contrastive learning with augmentations. In *NeurIPS*, 2020.

Junliang Yu, Hongzhi Yin, Jundong Li, Qinyong Wang, Nguyen Quoc Viet Hung, and Xiangliang Zhang. Self-supervised multi-channel hypergraph convolutional network for social recommendation. In *WWW*, 2021.

Manzil Zaheer, Satwik Kottur, Siamak Ravanbakhsh, Barnabas Poczos, Russ R Salakhutdinov, and Alexander J Smola. Deep sets. In *NeurIPS*, 2017.

Chuxu Zhang, Dongjin Song, Chao Huang, Ananthram Swami, and Nitesh V Chawla. Heterogeneous graph neural network. In *KDD*, 2019.

Junwei Zhang, Min Gao, Junliang Yu, Lei Guo, Jundong Li, and Hongzhi Yin. Double-scale self-supervised hypergraph learning for group recommendation. In *CIKM*, 2021.

Yizhen Zheng, Shirui Pan, Vincent Lee, Yu Zheng, and Philip S Yu. Rethinking and scaling up graph contrastive learning: An extremely efficient approach with group discrimination. In *NeurIPS*, 2022.

A APPENDIX

In this section, we provide a proof of each theorem. For notational simplicity, we denote the conditional probability of A given B, which is originally denote as $p\left(A \mid B\right)$, as $p(A : B)$.

A.1 PROOF OF THEOREM 1

Proof. We first analyze a node v_i that belongs to C_1 (i.e., $v_i \in C_1$). By definition, $\mathbb{E}_{\boldsymbol{x}}[\mathbf{1}_{\mathcal{F}(\boldsymbol{x}_i)=1}] = P_{\boldsymbol{x}}\left(f(\boldsymbol{x}_i; \boldsymbol{\mu}_1, \mathbf{I}) > f(\boldsymbol{x}_i; \boldsymbol{\mu}_0, \mathbf{I})\right)$ holds. Thus, $\mathbb{E}_{\boldsymbol{x}}[\mathbf{1}_{\mathcal{F}(\boldsymbol{x}_i)=1}]$ is determined by the distribution of $f(\boldsymbol{x}_i; \boldsymbol{\mu}_1, \mathbf{I}) > f(\boldsymbol{x}_i; \boldsymbol{\mu}_0, \mathbf{I})$, where a random variable is $\boldsymbol{x}_i$. The exact formula of this inequality is derived as follows:

$$
\begin{aligned}
& f(\boldsymbol{x}_i; \boldsymbol{\mu}_1, \mathbf{I}) > f(\boldsymbol{x}_i; \boldsymbol{\mu}_0, \mathbf{I}), \\
\equiv & \exp(-(\boldsymbol{x}_i - \boldsymbol{\mu}_1)^T(\boldsymbol{x}_i - \boldsymbol{\mu}_1)) > \exp(-(\boldsymbol{x}_i - \boldsymbol{\mu}_0)^T(\boldsymbol{x}_i - \boldsymbol{\mu}_0)), \\
\equiv & (\boldsymbol{x}_i - \boldsymbol{\mu}_1)^T(\boldsymbol{x}_i - \boldsymbol{\mu}_1) < (\boldsymbol{x}_i - \boldsymbol{\mu}_0)^T(\boldsymbol{x}_i - \boldsymbol{\mu}_0), \\
= & \boldsymbol{x}_i^T\boldsymbol{x}_i - 2\boldsymbol{\mu}_1^T\boldsymbol{x}_i + \boldsymbol{\mu}_1^T\boldsymbol{\mu}_1 < \boldsymbol{x}_i^T\boldsymbol{x}_i - 2\boldsymbol{\mu}_0^T\boldsymbol{x}_i + \boldsymbol{\mu}_0^T\boldsymbol{\mu}_0, \\
\equiv & (\boldsymbol{\mu}_1 - \boldsymbol{\mu}_0)^T\boldsymbol{x}_i + \boldsymbol{\mu}_0^T\boldsymbol{\mu}_0 - \boldsymbol{\mu}_1^T\boldsymbol{\mu}_1 > 0 \equiv \vec{\mathbf{1}}^T\boldsymbol{x}_i > 0, \quad \because \text{definition of } \boldsymbol{\mu}_1 \text{ and } \boldsymbol{\mu}_0 \text{ in Assumption 1.}
\end{aligned}
$$

Thus, $\mathbb{E}_{\boldsymbol{x}}[\mathbf{1}_{\mathcal{F}(\boldsymbol{x}_i)=1}]$ is equivalent to $P_{\boldsymbol{x}}(\vec{\mathbf{1}}^T\boldsymbol{x}_i > 0)$. In a similar sense, $\mathbb{E}_{\boldsymbol{x}}[\mathbf{1}_{\mathcal{F}(\boldsymbol{z}_i)=1}]$ is equivalent to $P_{\boldsymbol{x}}(\vec{\mathbf{1}}^T\boldsymbol{z}_i > 0)$, since as mentioned in Section 3.2, $\boldsymbol{z}_i$ is a function of $\boldsymbol{x}_k, \forall v_k \in \mathcal{V}$.

Now, we present an exact form of $\boldsymbol{z}_i$. Since $\boldsymbol{z}_i = \boldsymbol{x}_i - \gamma\nabla_{\boldsymbol{x}_i}\mathcal{L}$ holds by (**F2**), we first induce $\nabla_{\boldsymbol{x}_i}\mathcal{L}$:

$$
\begin{aligned}
\nabla_{\boldsymbol{x}_i}\mathcal{L} &= \frac{\partial\left(-\log(p_{(\mathbf{X},\mathcal{E},\Theta)}\left(v_i : q_{ij}\right))\right)}{\partial \boldsymbol{x}_i} = \frac{\partial\left(-\log\left(\frac{\exp(\boldsymbol{x}_i^T(\sum_{v_k\in q_{ij}}\boldsymbol{x}_k))}{\sum_{v_t\in\mathcal{V}}\exp(\boldsymbol{x}_t^T(\sum_{v_k\in q_{ij}}\boldsymbol{x}_k))}\right)\right)}{\partial \boldsymbol{x}_i}, && (6) \\
&= -\frac{\partial\left(\boldsymbol{x}_i^T(\sum_{v_k\in q_{ij}}\boldsymbol{x}_k)\right)}{\partial \boldsymbol{x}_i} + \frac{\partial\left(\log\left(\sum_{v_t\in\mathcal{V}}\exp(\boldsymbol{x}_t^T(\sum_{v_k\in q_{ij}}\boldsymbol{x}_k))\right)\right)}{\partial \boldsymbol{x}_i}, && (7) \\
&= -\left(\sum_{v_k\in q_{ij}}\boldsymbol{x}_k\right) + \frac{\exp(\boldsymbol{x}_i^T(\sum_{v_k\in q_{ij}}\boldsymbol{x}_k))}{\sum_{v_t\in\mathcal{V}}\exp(\boldsymbol{x}_t^T(\sum_{v_k\in q_{ij}}\boldsymbol{x}_k))}\left(\sum_{v_k\in q_{ij}}\boldsymbol{x}_k\right), && (8) \\
&= -\left(1 - \frac{\exp(\boldsymbol{x}_i^T(\sum_{v_k\in q_{ij}}\boldsymbol{x}_k))}{\sum_{v_t\in\mathcal{V}}\exp(\boldsymbol{x}_t^T(\sum_{v_k\in q_{ij}}\boldsymbol{x}_k))}\right)\left(\sum_{v_k\in q_{ij}}\boldsymbol{x}_k\right). && (9)
\end{aligned}
$$

By Eq (9), $\boldsymbol{z}_i$ can be expressed as a function of $\boldsymbol{x}_k, \forall v_k \in \mathcal{V}$, as follows:

$$
\boldsymbol{z}_i = \boldsymbol{x}_i + \gamma\underbrace{\left(1 - \frac{\exp(\boldsymbol{x}_i^T(\sum_{v_k\in q}\boldsymbol{x}_k))}{\sum_{v_t\in\mathcal{V}}\exp(\boldsymbol{x}_t^T(\sum_{v_k\in q}\boldsymbol{x}_k))}\right)}_{\text{(Term 1)}}\left(\sum_{v_k\in q}\boldsymbol{x}_k\right). \tag{10}
$$

Let $\boldsymbol{x}'_q$ denotes $\sum_{v_k\in q_{ij}}\boldsymbol{x}_k$. Furthermore, denote (Term 1) in Eq (10) as $f(\boldsymbol{x}) \in (0, 1)$. Then, we rewrite Eq (10) as $\boldsymbol{z}_i = \boldsymbol{x}_i + \gamma\left(1 - f(\boldsymbol{x})\right)\boldsymbol{x}'_q$. We finally rewrite $\vec{\mathbf{1}}^T\boldsymbol{z}_i$ as follows:

$$
\vec{\mathbf{1}}^T\boldsymbol{z}_i = \vec{\mathbf{1}}^T\boldsymbol{x}_i + \gamma(1 - f(\boldsymbol{x}))\vec{\mathbf{1}}^T\boldsymbol{x}'_q. \tag{11}
$$

Let β denotes $\vec{\mathbf{1}}^T\boldsymbol{x}'_q$. Note that by the statement of Theorem 1, $\vec{\mathbf{1}}^T\boldsymbol{x}'_q > 0 \equiv \beta > 0$ holds. Thus, our main interest, which is $P_{\boldsymbol{x}}(\vec{\mathbf{1}}^T\boldsymbol{z}_i > 0)$, can be rewritten as follows:

$$
P_{\boldsymbol{x}}\left(\vec{\mathbf{1}}^T\boldsymbol{z}_i > 0\right) = P_{\boldsymbol{x}}\left(\left(\vec{\mathbf{1}}^T\boldsymbol{x}_i + \gamma(1 - f(\boldsymbol{x}))\beta\right) > 0\right). \tag{12}
$$

Note that when $\vec{\mathbf{1}}^T \boldsymbol{x}_i > 0$ holds, $\vec{\mathbf{1}}^T \boldsymbol{z}_i > 0$ holds as well, since $\gamma(1 - f(\boldsymbol{x}))\beta > 0$ holds. Thus, Eq (12) is split as follows:

$$P_{\boldsymbol{x}}\left(\vec{\mathbf{1}}^T \boldsymbol{z}_i > 0\right) = P_{\boldsymbol{x}}\left(\vec{\mathbf{1}}^T \boldsymbol{x}_i > 0\right) + P_{\boldsymbol{x}}\left(-\gamma(1 - f(\boldsymbol{x}))\beta < \vec{\mathbf{1}}^T \boldsymbol{x}_i < 0\right),$$

$$= \mathbb{E}_{\boldsymbol{x}}[\mathbf{1}_{\mathcal{F}(\boldsymbol{z}_i)=1}] = \underbrace{\mathbb{E}_{\boldsymbol{x}}[\mathbf{1}_{\mathcal{F}(\boldsymbol{x}_i)=1}]}_{\text{(a) Expected accuracy of naive } \boldsymbol{x}_i} + \underbrace{P_{\boldsymbol{x}}\left(-\gamma\beta < \frac{\vec{\mathbf{1}}^T \boldsymbol{x}_i}{(1 - f(\boldsymbol{x}))} < 0\right)}_{\text{(b) Additional gain via hyperedge filling}}. \tag{13}$$

Note that the gain term, which is the (b) term of Eq (13), is always greater than zero.

Generalizing to $v_i \in C_0$. Now, we analyze a node v_i that belongs to C_0 (i.e., $v_i \in C_0$). In this case, the previous condition $\vec{\mathbf{1}}^T \boldsymbol{x}'_q > 0 \equiv \beta > 0$ becomes $\vec{\mathbf{1}}^T \boldsymbol{x}'_q < 0 \equiv \beta < 0$. In a similar sense, for the expected accuracy: $P_{\boldsymbol{x}}\left(\vec{\mathbf{1}}^T \boldsymbol{z}_i > 0\right)$ is changed as $P_{\boldsymbol{x}}\left(\vec{\mathbf{1}}^T \boldsymbol{z}_i < 0\right)$. In this setting, we can directly extend the result of Eq (12) as follows:

$$P_{\boldsymbol{x}}\left(\vec{\mathbf{1}}^T \boldsymbol{z}_i < 0\right) = P_{\boldsymbol{x}}\left(\left(\vec{\mathbf{1}}^T \boldsymbol{x}_i + \gamma(1 - f(\boldsymbol{x}))\beta\right) < 0\right). \tag{14}$$

By employing the above proof, we can obtain the following result (note that $\beta < 0$ in this case):

$$P_{\boldsymbol{x}}\left(\vec{\mathbf{1}}^T \boldsymbol{z}_i < 0\right) = P_{\boldsymbol{x}}\left(\vec{\mathbf{1}}^T \boldsymbol{x}_i < 0\right) + P_{\boldsymbol{x}}\left(0 < \vec{\mathbf{1}}^T \boldsymbol{x}_i < -\gamma(1 - f(\boldsymbol{x}))\beta\right),$$

$$= \mathbb{E}_{\boldsymbol{x}}[\mathbf{1}_{\mathcal{F}(\boldsymbol{z}_i)=0}] = \underbrace{\mathbb{E}_{\boldsymbol{x}}[\mathbf{1}_{\mathcal{F}(\boldsymbol{x}_i)=0}]}_{\text{(a) Expected accuracy of naive } \boldsymbol{x}_i} + \underbrace{P_{\boldsymbol{x}}\left(-\gamma\beta < \frac{\vec{\mathbf{1}}^T \boldsymbol{x}_i}{(1 - f(\boldsymbol{x}))} < 0\right)}_{\text{(b) Additional gain via hyperedge filling}}. \tag{15}$$

Thus, we can derive the same result for $v_i \in C_0$ also. □

A.2 Proof of Theorem 2.

Remark. *We have denoted the homophilic ratio in Assumption 2 as $\mathcal{P}$ to distinguish it from the hyperedge filling probability $p_{(\mathbf{X},\mathcal{E},\Theta)}$. In this proof, by allowing a slight duplication in notation, we let $\mathcal{P} := p$, since we do not use $p_{(\mathbf{X},\mathcal{E},\Theta)}$ in this proof. In addition, we let $e_j := e$ and $q_{ij} := q$.*

Proof. We first derive the functional form of $P_{\boldsymbol{x},e}\left(\vec{\mathbf{1}}^T\left(\sum_{v_k \in q} \boldsymbol{x}_k\right) > 0 : p\right)$. By the condition of the theorem such that $v_i \in e_j \cap C_1$, the following holds:

$$P_{\boldsymbol{x},e}\left(\vec{\mathbf{1}}^T\left(\sum_{v_k \in q} \boldsymbol{x}_k\right) > 0 : p\right) = \frac{P_{\boldsymbol{x},e}\left(\vec{\mathbf{1}}^T\left(\sum_{v_k \in q} \boldsymbol{x}_k\right) > 0, v_i \in e : p\right)}{P_e\left(v_i \in e : p\right)}. \tag{16}$$

It is important to note that if the number of nodes that belong to both C_1 and e_j is decided, denoted by s (i.e., $s = |e \cap C_1|$), the distribution of $\vec{\mathbf{1}}^T\left(\sum_{v_k \in q} \boldsymbol{x}_k\right)$ is automatically decided, since $\boldsymbol{x}_t, \forall v_t \in \mathcal{V}$ is independently generated from Gaussian distribution, whose mean vector is decided according to the class of the corresponding node. This is because for a given s, and by letting the size of the hyperedge e as S (i.e., $|e| = S$), $\sum_{v_k \in q} \boldsymbol{x}_k \sim \mathcal{N}((2s - 1 - S)\boldsymbol{\mu}_1, (S-1)\mathbf{I})$ holds. From this result, the following two results are induced:

$$\vec{\mathbf{1}}^T\left(\sum_{v_k \in q} \boldsymbol{x}_k\right) \sim \mathcal{N}\left(\frac{(2s - 1 - S)d}{2}, (S-1)d\right), \tag{17}$$

$$P_{\boldsymbol{x}}\left(\vec{\mathbf{1}}^T\left(\sum_{v_k \in q} \boldsymbol{x}_k\right) > 0 : s\right) = \Phi\left((2s - S - 1)\sqrt{\frac{d}{4(S-1)}}\right). \tag{18}$$

Thus, we rewrite Eq (16) as follows:

$$\equiv \sum_{s=0}^{S} \frac{P_{\boldsymbol{x},e}\left(\vec{\mathbf{1}}^T\left(\sum_{v_k\in q}\boldsymbol{x}_k\right)>0, s, v_i\in e\right)}{P_e\left(v_i\in e:p\right)}, \tag{19}$$

$$= \sum_{s=0}^{S} \frac{P_{\boldsymbol{x}}\left(\vec{\mathbf{1}}^T\left(\sum_{v_k\in q}\boldsymbol{x}_k\right)>0:s\right)\times P_e(s, v_i\in e)}{P_e\left(v_i\in e:p\right)}. \tag{20}$$

By Assumption 2, each $P_e(s, v_i \in e)$ is derived as follows[7]:

$$P_e(s, v_i\in e:p) = \binom{S}{s}\left(\underbrace{\frac{p^s(1-p)^{S-s}}{2}}_{\text{prob. of } s \text{ at } c=1} + \underbrace{\frac{(1-p)^s p^{S-s}}{2}}_{\text{prob. of } s \text{ at } c=0}\right)\underbrace{\left(1-\frac{\binom{N-1}{s}}{\binom{N}{s}}\right)}_{\text{prob. of } v_i\in C_1\cap e}. \tag{21}$$

By using Eq (21), we derive $P_e(v_i \in e : p)$ as follows:

$$P_e(v_i\in e:p) = \sum_{s=0}^{S}\binom{S}{s}\left(\frac{p^s(1-p)^{S-s}}{2}+\frac{(1-p)^s p^{S-s}}{2}\right)\left(1-\frac{\binom{N-1}{s}}{\binom{N}{s}}\right), \tag{22}$$

$$= \sum_{s=0}^{S}\binom{S}{s}\left(\frac{p^s(1-p)^{S-s}}{2}+\frac{(1-p)^s p^{S-s}}{2}\right)\frac{s}{N}, \tag{23}$$

$$= \frac{1}{N}\sum_{s=0}^{S}\binom{S}{s}\left(\underbrace{\frac{sp^s(1-p)^{S-s}}{2}}_{s\sim B(S,p)}+\underbrace{\frac{s(1-p)^s p^{S-s}}{2}}_{s\sim B(S,1-p)}\right), \tag{24}$$

$$= \frac{1}{N}\left(\frac{Sp}{2}+\frac{S(1-p)}{2}\right), \because \text{ each is an expectation function,} \tag{25}$$

$$= \frac{S}{2N}. \tag{26}$$

With the result of Eq (26) and Eq (18), we rewrite Eq (20) as follows:

$$\equiv \frac{2N}{S}\sum_{s=0}^{S}\binom{S}{s}\left(\frac{p^s(1-p)^{S-s}}{2}+\frac{(1-p)^s p^{S-s}}{2}\right)\frac{s}{N}\Phi\left((2s-1-S)\sqrt{\frac{d}{4(S-1)}}\right), \tag{27}$$

$$= \frac{1}{S}\sum_{s=0}^{S}\binom{S}{s}s\left(p^s(1-p)^{S-s}+(1-p)^s p^{S-s}\right)\Phi\left((2s-1-S)\sqrt{\frac{d}{4(S-1))}}\right). \tag{28}$$

Note that our main function, which is $P_{\boldsymbol{x},e}\left(\vec{\mathbf{1}}^T\left(\sum_{v_k\in q}\boldsymbol{x}_k\right)>0:p\right)$, is equal to Eq (28). Here, one can easily verify that Eq (28) is equivalent to the first statement of the theorem.

Now, we show the first and second statements of the theorem. Here, we first show the second statement, and from the result, we further prove the first statement.

Second statement. Now, we further rewrite Eq (28) by adequately mixing two binomial functions. For simplicity, we denote $\Phi((2s-1-S)\sqrt{\frac{d}{4(S-1)}})$ as $\phi(s)$, since $\Phi(\cdot)$ only depends on s, and other terms are fixed constants. We rewrite Eq (28) as follows:

$$= \frac{1}{S}\sum_{s=0}^{S}\binom{S}{s}s\left(p^s(1-p)^{S-s}+(1-p)^s p^{S-s}\right)\phi(s), \tag{29}$$

$$= \underbrace{\frac{1}{S}\sum_{s=0}^{S}\binom{S}{s}sp^s(1-p)^{S-s}\phi(s)}_{\text{(Term 1)}} + \underbrace{\frac{1}{S}\sum_{s=0}^{S}\binom{S}{s}s(1-p)^s(p)^{S-s}\phi(s)}_{\text{(Term 2)}}. \tag{30}$$

[7] prob. indicates probability.

We define $s' := (S - s)$. Due to the symmetric characteristic of the binomial function and standard Gaussian distribution, we can rewrite (Term 2) in Eq (30) as follows:

$$\equiv \frac{1}{S}\sum_{s'=0}^{S}\binom{S}{s'}p^{s'}(1-p)^{S-s'}(S-s')\Phi\left((S-2s'-1)\sqrt{\frac{d}{4(S-1)}}\right). \tag{31}$$

Since we can regard s and s' as equivalent terms in our framework, we add (Term 1) of Eq (30) and Eq (31) as follows:

$$= \frac{1}{S}\sum_{s=0}^{S}\binom{S}{s}p^{s}(1-p)^{S-s}\underbrace{\left[(S-s)\Phi\left((S-2s-1)\sqrt{\frac{d}{4(S-1)}}\right)+s\Phi\left((2s-S-1)\sqrt{\frac{d}{4(S-1)}}\right)\right]}_{\text{Term (a)}}. \tag{32}$$

We aim to show that Eq (32) is a strictly increasing function w.r.t. $p \in [0.5, 1]$. For simplicity, we let $K := \sqrt{d/(4(S-1))}$. We first discard $1/(S+1)$ from Eq (32) for simplicity, since $1/(S+1)$ is a constant, which is independent of the increasing/decreasing of values. When we do not consider Eq (32) Term (a), Eq (32) is equivalent to 1, and this is a probability distribution of binomial distribution.

That is, we can think of Eq (32) as a weighted average of the following values:

$$\left[(S-s)\Phi\left((S-2s-1)K\right)+s\Phi\left((2s-S-1)K\right)\right], \forall s \in \{0, 1, \cdots, S\}. \tag{33}$$

Specifically, we denote $\binom{S}{s}p^{s}(1-p)^{S-s}$ as a weight of $\left[(S-s)\Phi\left((S-2s-1)K\right)+s\Phi\left((2s-S-1)K\right)\right]$. Note that values of Eq (33) and their weights are both symmetric about $s = S/2$: s and $S-s$ have the same value. Thus, we can rewrite Eq (32) for an even number S as:

$$\begin{aligned}\equiv &\sum_{s=\lfloor S/2\rfloor}^{S}\binom{S}{s}\left(p^{s}(1-p)^{S-s}+(1-p)^{s}p^{S-s}\right)\\ &\times\left[(S-s)\Phi\left((S-2s-1)K\right)+s\Phi\left((2s-S-1)K\right)\right].\end{aligned} \tag{34}$$

While this formulation is for an odd number S, we can extend further results to an even number S.

We first show that Eq (33) is an increasing function w.r.t. $s \in \{\lfloor S/2\rfloor, \lfloor S/2\rfloor+1, \cdots, S\}$. For two cases where $s = k$ and $s = k+1$, their Eq (33) is compared as follows:

$$\left[(S-k-1)\Phi\left(S-2k-3\right)+(k+1)\Phi\left(2k-S+1\right)\right] \tag{35}$$

$$>\left[(S-k)\Phi\left(S-2k-1\right)+k\Phi\left(2k-S-1\right)\right], \tag{36}$$

$$\equiv k\left(\Phi\left(2k-S+1\right)-\Phi\left(2k-S-1\right)\right)+\Phi\left(2k-S+1\right) \tag{37}$$

$$>(S-k)\left(\Phi\left(S-2k-1\right)-\Phi\left(S-2k-3\right)\right)+\Phi\left(S-2k-3\right), \tag{38}$$

By the condition of $s \geq \lfloor S/2\rfloor$, $k > S-k$ holds. Furthermore, by the characteristic of the CDF of standard normal distribution, $\left(\Phi\left(2k-S+1\right)-\Phi\left(2k-S-1\right)\right) > \left(\Phi\left(S-2k-1\right)-\Phi\left(S-2k-3\right)\right)$ holds. Moreover, since $s \geq \lfloor S/2\rfloor$, $\Phi\left(2k-S+1\right) > \Phi\left(S-2k-3\right)$ also holds. In sum, Eq (35) > Eq (36) holds, and this result implies that Eq (33) is an increasing function w.r.t. $s \in \{\lfloor S/2\rfloor, \lfloor S/2\rfloor+1, \cdots, S\}$.

Since greater s has a higher value of Eq (33), we can naturally conclude that Eq (34), which is our goal function, is an increasing function w.r.t. p if weights are more assigned to the terms related to the higher s as p increases. This idea is formalized as: $\exists s^* \in \{\lfloor S/2\rfloor, \cdots, S\}$, s.t. $\partial w(p,s)/\partial p > 0, \forall s \geq s^*$ and $\partial w(p,s)/\partial p < 0, \forall s \leq s^*$, where $w(p,s) = \binom{S}{s}\left(p^{s}(1-p)^{S-s}+(1-p)^{s}p^{S-s}\right)$. To this end, we derive the first derivative of $w(p,s)$:

$$\frac{\partial\omega(p,s)}{\partial p} = \binom{S}{s}\Big(\underbrace{sp^{s-1}(1-p)^{S-s}}_{(a)}-\underbrace{(S-s)p^{s}(1-p)^{S-s-1}}_{(b)} \tag{39}$$

$$-\underbrace{s(1-p)^{s-1}p^{S-s}}_{(c)}+\underbrace{(S-s)(1-p)^{s}p^{S-s-1}}_{(d)}\Big). \tag{40}$$

We then compute $(a)+(b)$ and $(c)+(d)$ respectively, and sum them up as follows:

$$(a)+(b) = p^{s-1}(1-p)^{S-s-1}(s(1-p)-(S-s)p), \tag{41}$$
$$= p^{s-1}(1-p)^{S-s-1}(s-sp-Sp+sp), \tag{42}$$
$$(c)+(d) = (1-p)^{s-1}p^{S-s-1}(-sp+(S-s)(1-p)), \tag{43}$$
$$= (1-p)^{s-1}p^{S-s-1}(-sp+(S-s)-Sp+sp), \tag{44}$$
$$(a)+(b)+(c)+(d) = p^{s-1}(1-p)^{S-s-1}(s-Sp)+(1-p)^{s-1}p^{S-s-1}(S-s-Sp). \tag{45}$$

Remark. *When $p = 1/2$, Eq (45) $= 0$ holds, which means that if Eq (32) turns out to be an increasing function w.r.t. p, Eq (32) has its minimum value at $p = 1/2$. Thus, we narrow down the range of p as $p > 1/2$.*

Moving on to our main object, first, we find s^* such that Eq (45) $= 0$ holds. We utilize the logarithm function to simplify the computation (note that $\binom{S}{s}$ is canceled out).

$$\equiv p^{(s-1)}(1-p)^{S-s-1}(s-Sp) = (1-p)^{(s-1)}p^{S-s-1}(s-S+Sp), \tag{46}$$
$$\equiv (s-1)\log p + (S-s-1)\log(1-p) + \log(s-Sp) =$$
$$(s-1)\log(1-p) + (S-s-1)\log p + \log(s-S+Sp),$$
$$= (s-1)\log(\frac{p}{1-p}) + (S-s-1)\log\frac{1-p}{p} + \log\frac{s-Sp}{s-S(1-p)} = 0,$$
$$= \underbrace{(2s-S)\log\frac{p}{1-p}}_{\text{Term (a)}} + \underbrace{\log\frac{s-Sp}{s-S(1-p)}}_{\text{Term (b)}} = 0. \tag{47}$$

However, it is hard to obtain the exact solution of Eq (47). Instead, we analyze the formula of Term (a) + Term (b) in Eq (47), which is expressed as below:

$$(2s-S)\log\frac{p}{1-p} + \log\frac{s-Sp}{s-S(1-p)}. \tag{48}$$

To show the required conditions, it is enough to show that Eq (48) < 0 holds at $s = S/2$, and Eq (48) > 0 holds at $s = S$. This is because since Eq (48) is an increasing function w.r.t. s, the above two conditions imply that there exists a s^*, which is our interest, between $S/2$ and S. Thus, we finalize the proof by showing that at $s = S/2$, Eq (48) < 0 holds and at $s = S$, Eq (48) > 0 holds.

When plugging $S/2$ to s, $2s - S$ gets zero. Since $p > 1/2$ is given, $\log\frac{s-Sp}{s-S(1-p)}$ becomes negative. Thus, we have demonstrated the first claim. We now plug S into s and obtain the following result:

$$\equiv (2S-S)\log\frac{p}{1-p} + \log\frac{S-Sp}{S-S(1-p)} > 0, \tag{49}$$
$$\equiv S\log\frac{p}{1-p} + \log\frac{S(1-p)}{Sp} > 0, \tag{50}$$
$$\equiv S\log\frac{p}{1-p} - \log\frac{p}{1-p} > 0, \tag{51}$$
$$\equiv (S-1)\log\frac{p}{1-p} > 0. \tag{52}$$

Thus, we can conclude that Eq (32), which is our interest, is an increasing function w.r.t. $p > 1/2$, and has its minimum value at $p = 1/2$.

Now, we show that the above proof can also be applied to an even number S. Note that for an even number S, Eq (32) is equal to the addition of Eq (34) that starts with $s = S/2 + 1$ and Eq (53),

$$w(p,s) = \binom{S}{\frac{S}{2}} \times \frac{S}{2} \times p^{\frac{S+1}{2}}(1-p)^{\frac{S+1}{2}}. \tag{53}$$

Specifically, if we obtain $\partial w(p,s)/\partial p$, we get

$$\frac{\partial w(p,s)}{\partial p} = \left(\binom{S}{\frac{S}{2}} \times \frac{S}{2}\right) \times \left(\frac{S}{2} p^{\frac{S-2}{2}} (1-p)^{\frac{S-2}{2}} (1-2p)\right) \leq 0, \forall p \in [0.5, 1]. \tag{54}$$

Since the sign of $\partial w(p,s)/\partial w(p,s)$ remains unchanged for $s = S + 1/2$, our proof is still valid for an even number S.

First statement. From the above proof, we now show the lower bound of Eq (27), which is the first statement. As described on Remark in A.2, the value of Eq (27) (equivalent to Eq (32)) is minimized at $p = 0.5$. Thus, we show the statement by finding the lower bound of Eq (28) at $p = 0.5$, by again denoting $K := \sqrt{\frac{d}{4(S-1)}}$, as follows:

$$= \frac{1}{S} \sum_{s=0}^{S} \binom{S}{s} s \left(p^s (1-p)^{S-s} + (1-p)^s p^{S-s}\right) \Phi\left((2s-1-S)\sqrt{\frac{d}{4(S-1))}}\right), \tag{55}$$

$$= \frac{1}{S} \sum_{s=0}^{S} \binom{S}{s} 2s \left(\frac{1}{2}\right)^S \Phi\left((2s-S-1)K\right). \tag{56}$$

First, consider an even number S. Then, for $\Phi((2s-S-1)K), \forall s \in \{1, \cdots, S\}$, consider the below relations:

$$1 \underbrace{\Phi(-S+1)}_{(a1)} + 2 \underbrace{\Phi(-S+3)}_{(b1)} + \cdots + (S-1) \underbrace{\Phi(S-3)}_{(b2)} + S \underbrace{\Phi(S-1)}_{(a2)}. \tag{57}$$

In Eq (57), $(a1) + (a2) = 1$ holds, and $(b1) + (b2) = 1$ holds also. In this manner, we can pair all terms in Eq 57. If we take a closer look at this, pairs have a relation of: $k_{11}k_{12} + k_{21}k_{22}$ such that $k_{11} + k_{21} = S, k_{12} + k_{22} = 1$, $k_{11} < k_{12}$, and $k_{21} < k_{22}$ hold. Note that $k_{11}k_{12} + k_{21}k_{22}$ is lower-bounded by $\frac{k_{11}+k_{21}}{2}$ since distributing the weight of a larger value to a smaller value will decrease the overall value. From this result, we can obtain a lower bound of Eq (57) as follows:

$$\frac{1}{S} \sum_{s=0}^{S} \binom{S}{s} 2s \left(\frac{1}{2}\right)^S \Phi\left((2s-S-1)K\right) \geq \frac{1}{S} \sum_{s=0}^{S} \binom{S}{s} 2s \left(\frac{1}{2}\right)^S \frac{1}{2} = 0.5. \tag{58}$$

Now, we consider an odd number S. Similar things also happen in this case, but there is a term $s = \frac{S+1}{2}; \Phi(0)$ that does not have any pair. On the other hand, since $\Phi(0) = 0.5$, we can still ensure Eq (58) holds in this case. Thus, we have derived that regardless of the fact whether S is an odd or even number, Eq (28) at $p = 0.5$ is lower-bounded by 0.5, which is a global lower bound of Eq (28). Thus, the first statement has been proven.

Generalization to $v_i \in C_0$. Note that the required condition for the improvement in $v_i \in C_0$ is $\mathbf{1}^T \sum_{v_k \in q} \boldsymbol{x}_k < 0$. Thus, we further investigate $P_{\boldsymbol{x},e}\left(\mathbf{1}^T \sum_{v_k \in q} \boldsymbol{x}_k < 0 \;\middle|\; \mathcal{P}\right)$, where $v_i \in e$ and $q = e \setminus \{v_i\}$ (refer to Remark). First, let s denote the number of nodes that belong to both e_j and C_0. Note that we aim to investigate the following probability:

$$P_{\boldsymbol{x},e}\left(\vec{\mathbf{1}}^T \left(\sum_{v_k \in q} \boldsymbol{x}_k\right) < 0 : p\right) = \frac{P_{\boldsymbol{x},e}\left(\vec{\mathbf{1}}^T \left(\sum_{v_k \in q} \boldsymbol{x}_k\right) < 0, v_i \in e : p\right)}{P_e\left(v_i \in e : p\right)}. \tag{59}$$

Here, the following holds:

$$\sum_{v_k \in q} \boldsymbol{x}_k \sim \mathcal{N}((2s-1-S)\boldsymbol{\mu}_0, (S-1)\mathbf{I}), \tag{60}$$

$$\vec{\mathbf{1}}^T \left(\sum_{v_k \in q} \boldsymbol{x}_k\right) \sim \mathcal{N}\left(-\frac{(2s-1-S)d}{2}, (S-1)d\right), \tag{61}$$

$$P_{\boldsymbol{x}}\left(\vec{\mathbf{1}}^T \left(\sum_{v_k \in q} \boldsymbol{x}_k\right) < 0 : s\right) = \Phi\left((2s-S-1)\sqrt{\frac{d}{4(S-1)}}\right). \tag{62}$$

Note that Eq. (62) is equivalent to Eq. (18). Moreover, the following also holds:

$$P_e(s, v_i \in e : p) = \binom{S}{s} \left(\underbrace{\frac{p^s(1-p)^{S-s}}{2}}_{\text{prob. of } s \text{ at } c=0} + \underbrace{\frac{(1-p)^s p^{S-s}}{2}}_{\text{prob. of } s \text{ at } c=1} \right) \underbrace{\left(1 - \frac{\binom{N-1}{s}}{\binom{N}{s}} \right)}_{\text{prob. of } v_i \in C_0 \cap e}. \tag{63}$$

Here again, Eq. (21) is equivalent to Eq. (63). Finally, we can guarantee that Eq. (59) is as follows:

$$\equiv \sum_{s=0}^{S} \frac{P_{\boldsymbol{x}} \left(\vec{\mathbf{1}}^T \left(\sum_{v_k \in q} \boldsymbol{x}_k \right) > 0 : s \right) \times P_e(s, v_i \in e)}{P_e\left(v_i \in e : p\right)}, \tag{64}$$

$$\equiv \frac{2N}{S} \sum_{s=0}^{S} \binom{S}{s} \left(\frac{p^s(1-p)^{S-s}}{2} + \frac{(1-p)^s p^{S-s}}{2} \right) \frac{s}{N} \Phi \left((2s - 1 - S) \sqrt{\frac{d}{4(S-1)}} \right), \tag{65}$$

$$= \frac{1}{S} \sum_{s=0}^{S} \binom{S}{s} s \left(p^s(1-p)^{S-s} + (1-p)^s p^{S-s} \right) \Phi \left((2s - 1 - S) \sqrt{\frac{d}{4(S-1))}} \right). \tag{66}$$

Importantly, Eq. (66) is equal to Eq. (28). This result implies that Theorem 2 and its proof is generalizable to the case of $v_i \in C_0$ also.

□

A.3 Empirical demonstration on the proof.

To empirically validate the proof provided above, we have conducted toy experiments. We have considered every combination of $S \in \{2, 3, 4, 5, 6, 7, 8\}$, which is a size of e_j (i.e., $|e_j|$), and $d \in \{2, 3, 4, 5, 6, 7, 8\}$, which is a dimension of input feature $\boldsymbol{x}_i \in \mathbb{R}^d, \forall v_i \in \mathcal{V}$. Then, we visualize how Eq (27) varies w.r.t. S, d, and $\mathcal{P} \in [0, 1]$, which corresponds to the X-axis of each plot. As shown in Figure 3, for all cases, we can verify that the value of $P_{\boldsymbol{x},e} \left(\vec{\mathbf{1}}^T \left(\sum_{v_k \in q} \boldsymbol{x}_k \right) > 0 : \mathcal{P} \right)$ is strictly increasing w.r.t. $\mathcal{P} \in [0.5, 1]$ (statement 2), and the value of $P_{\boldsymbol{x},e} \left(\vec{\mathbf{1}}^T \left(\sum_{v_k \in q} \boldsymbol{x}_k \right) > 0 : \mathcal{P} \right)$ is lower bounded by 0.5 (statement 1). Thus, we can ensure that Theorem 2 is valid through empirical verification.

B Additional Theoretical Analysis

B.1 Existence of reasonable solutions in the hyperedge filling task

In this section, we investigate the existence of a reasonable solution in the proposed hyperedge filling task. To this end, we first formalize the concept of *the hyperedge filling task is solved*.

Definition 1 (Solved hyperedge filing task)**.** *For a hypergraph $G = (\mathcal{V}, \mathcal{E})$, the hyperedge filling task is solved when the following holds:*

$$p_{(\mathbf{X}, \mathcal{E}, \Theta)} \left(v_i \mid e_j \setminus \{v_i\} \right) > p_{(\mathbf{X}, \mathcal{E}, \Theta)} \left(v_k \mid e_j \setminus \{v_i\} \right),$$
$$\forall v_i \in e_j, \forall v_k \in \{v_s : \{v_s\} \cap (e_j \setminus \{v_i\}) \notin \mathcal{E}, v_s \in \mathcal{V}\}, , \forall e_j \in \mathcal{E}.$$

Roughly, Definition 1 implies that for all possible hyperedge filling cases in a hypergraph G, the probability of filling a correct node for a given query subset is always greater than that of filling a wrong node. It is important to note that our goal is to identify whether there exists a **reasonable solution**, not a trivial solution. Thus, we define the notion of a reasonable solution as follows:

Definition 2 (Reasonable solution)**.** *Let $\mathcal{Q} := \{e_j \setminus \{v_i\} : \forall v_i \in e_j, \forall e_j \in \mathcal{E}\}$. For a hypergraph $G = (\mathcal{V}, \mathcal{E})$, a reasonable solution of the hyperedge filling task is a pair of node representations $\mathbf{Z} \in \mathbb{R}^{|\mathcal{V}| \times d}$ and query set representations $\mathbf{Q} \in \mathbb{R}^{|\mathcal{Q}| \times d}$ such that:*

$$\boldsymbol{z}_i^T \boldsymbol{q}_j > \boldsymbol{z}_k^T \boldsymbol{q}_j,$$
$$\forall v_i \in S_j, \forall v_k \in \mathcal{V} \setminus S_j, \forall q_j \in \mathcal{Q}, \text{ where } S_j = \{v_s : (\{v_s\} \cap q_j \in \mathcal{E}) \wedge (v_s \notin q_j), v_s \in \mathcal{V}\}.$$

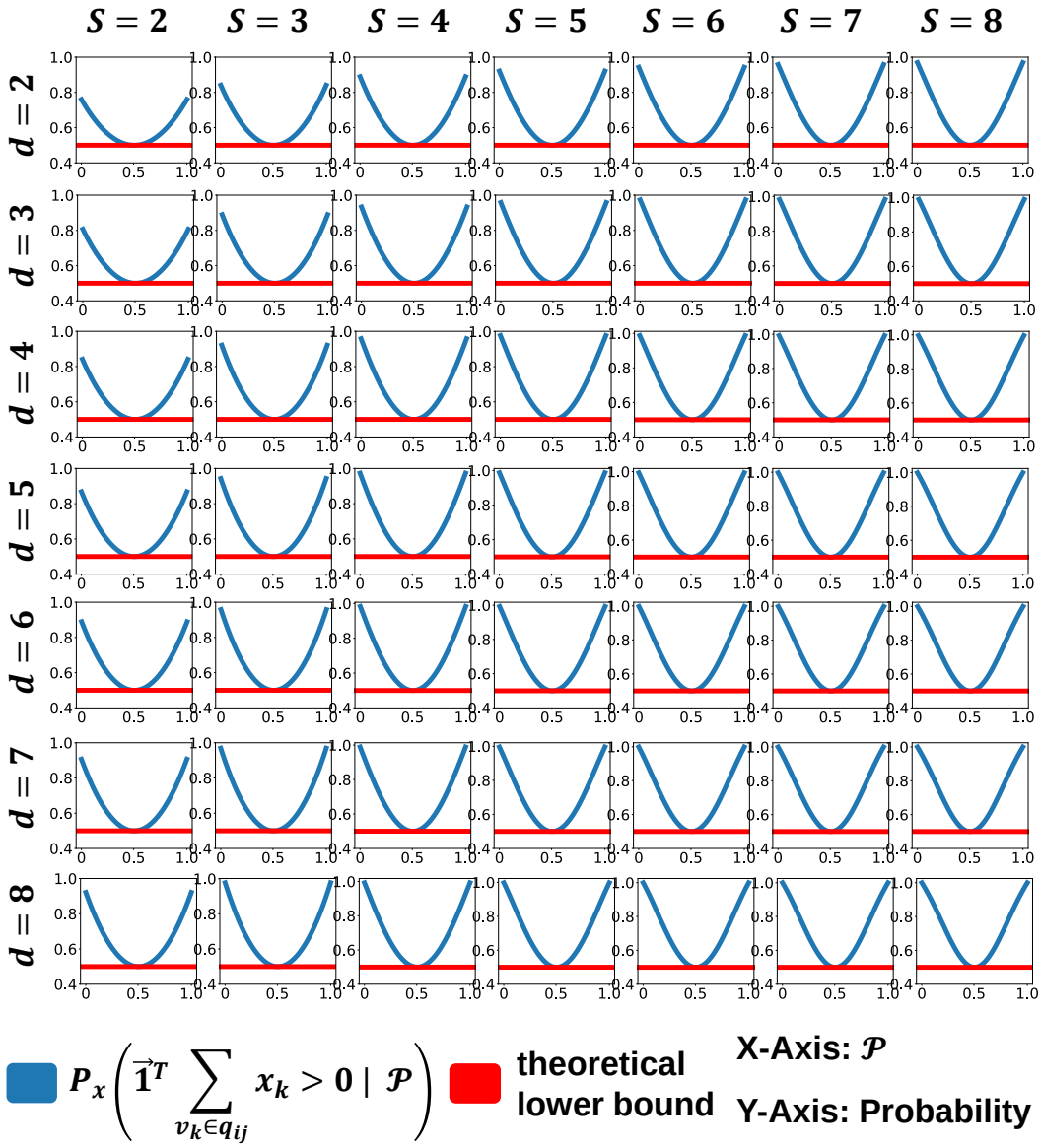

Figure 3: Empirical demonstration of Theorem 2. Note that S denotes the size of a hyperedge, and d denotes the dimension of features. As stated, $P_{\boldsymbol{x},e}\left(\vec{\mathbf{1}}^T\left(\sum_{v_k \in q} \boldsymbol{x}_k\right) > 0 : \mathcal{P}\right)$ is strictly increasing in $\mathcal{P} \in [0.5, 1]$ (statement 2), and lower bounded by 0.5 (statement 1).

Now, we analyze whether there exists a reasonable solution for any hypergraph $G = (\mathcal{V}, \mathcal{E})$.

Theorem 3 (Existence of a reasonable solution)**.** *For any hypergraph $G = (\mathcal{V}, \mathcal{E})$, there exists a reasonable solution for some embedding dimension d.*

Proof. Consider a binary matrix $\mathbf{B} \in \{1, 0\}^{|V| \times |\mathcal{Q}|}$, where each column $j \in \{1, \cdots, |\mathcal{Q}|\}$ represents one-hot encoding of S_j over $\mathcal{V}$ (i.e., $\mathbf{B}_{ij} = \mathbf{1}[v_i \in S_j]$, where $\mathbf{1}[\cdot]$ is an indicator function). Here, we can think of a matrix decomposition of $\mathbf{B}$, specifically, singular value decomposition of $\mathbf{B}$. Denote this singular value decomposition as $\mathbf{B} = \mathbf{U}\Sigma\mathbf{V}^T$, where $\mathbf{U} \in \mathbb{R}^{|\mathcal{V}| \times \text{rank}(\mathbf{B})}$, $\mathbf{V} \in \mathbb{R}^{\text{rank}(\mathbf{B}) \times \text{rank}(\mathbf{B})}$, and $\mathbf{V} \in \mathbb{R}^{|\mathcal{Q}| \times \text{rank}(\mathbf{B})}$. Let $\mathbf{Z} := \mathbf{U}\Sigma$ and $\mathbf{Q} := \mathbf{V}$. In such a case, the following holds:

$$\boldsymbol{z}_i^T \boldsymbol{q}_j = \begin{cases} 1 & \text{if } v_i \in S_j, \\ 0 & \text{otherwise.} \end{cases} \tag{67}$$

Thus, $\boldsymbol{z}_i^T \boldsymbol{q}_j > \boldsymbol{z}_k^T \boldsymbol{q}_j, \forall v_i \in S_j, \forall v_k \in \mathcal{V} \setminus S_j, \forall q_j \in \mathcal{Q}$ always holds, which implies that $\mathbf{Z} := \mathbf{U}\Sigma$ and $\mathbf{Q} := \mathbf{V}$ are one of reasonable solutions. □

From Theorem 3, we have demonstrated that there exists a reasonable solution for any hypergraph G. Thus, we can conclude that the hyperedge filling task has a solution all the time, and we are learning a solvable task.

B.2 Dimensional collapse of HypeBoy without projection heads.

In this subsection, we provide a theoretical analysis of why HypeBoy without head parameters may suffer from dimensional collapse. Jing et al. (2022) have suggested that one of the reasons for the dimensional collapse in contrastive learning lies in the gradient flow: the mechanism of how representations are updated via contrastive loss. Specifically, consider a linear model that creates representations of a n number of data by $\mathbf{Z} = \mathbf{X}\mathbf{W}$, where $\mathbf{X} \in \mathbb{R}^{n \times d}$ are node features and $\mathbf{W} \in \mathbb{R}^{d \times k}$ is a learnable parameter matrix. When we update parameters $\mathbf{W}$ by using contrastive losses, k-th biggest singular value of weight matrices σ_k evolve proportional to its own value (e.g., $\tilde{\sigma_k} \leftarrow \sigma_k \times c$, where $\tilde{\sigma_k}$ is a k-th biggest singular value of updated $\mathbf{W}$ and c is a positive constant). Due to this mechanism, small single values grow slowly or diminish, causing dimensional collapse.

In this analysis, motivated by the analysis of Jing et al. (2022), we track how singular values of representations change as we update representations via hyperedge filling. Following the setting of Jing et al. (2022), we consider a linear model: $\mathbf{Z} = \mathbf{X}\mathbf{W}$. Note that $\mathbf{X}$ are given features of data points. Thus, singular values of embeddings $\mathbf{Z}$ are dependent on $\mathbf{W}$.

We first define the loss of hyperedge filling as follows:

$$\mathcal{L} := -\sum_{e_j \in \mathcal{E}} \sum_{v_i \in e_j} \log \left(\frac{\exp\left(\boldsymbol{z}_i^T \left(\sum_{v_s \in q_{ij}} \boldsymbol{z}_s\right)\right)}{\sum_{v_t \in \mathcal{V}} \exp\left(\boldsymbol{z}_t^T \left(\sum_{v_s \in q_{ij}} \boldsymbol{z}_s\right)\right)} \right). \tag{68}$$

Now, we obtain the closed form of the following update equation, which is based on the gradient descent: $\mathbf{W} \leftarrow \mathbf{W} - \gamma \nabla_{\mathbf{W}} \mathcal{L}$, where γ is a fixed learning rate. We first derive $(\partial \mathcal{L} / \partial \mathbf{Z})$, and utilize the chain rule: $(\partial \mathcal{L} / \partial \mathbf{Z}) \times (\partial \mathbf{Z} / \partial \mathbf{W})$.

The derivative of numerators of Eq (68) can be written as follows:

$$-\frac{\partial \left(\sum_{e_j \in \mathcal{E}} \sum_{v_i \in e_j} \boldsymbol{z}_i^T \left(\sum_{v_s \in q_{ij}} \boldsymbol{z}_s\right)\right)}{\partial \mathbf{Z}} = -\mathbf{E}\mathbf{Z},$$
$$\text{where } \mathbf{E} \in \mathbb{R}^{|\mathcal{V}| \times |\mathcal{V}|}, \text{ s.t. } \mathbf{E}_{ij} = 2 \times |\{e_k : \{v_i, v_j\} \subseteq e_k, \forall e_k \in \mathcal{E}\}|.$$

We now derive the derivative of the denominators of Eq (68):

$$\frac{\partial \left(\sum_{e_j \in \mathcal{E}} \sum_{v_i \in e_j} \log \left(\sum_{v_t \in \mathcal{V}} \exp\left(\boldsymbol{z}_t^T \left(\sum_{v_s \in q_{ij}} \boldsymbol{z}_s\right)\right)\right)\right)}{\partial \mathbf{Z}}. \tag{69}$$

We denote a multiset of every possible subset of a hyperedge that a single node is omitted as $\mathcal{Q}$ (i.e., $\mathcal{Q} = \{e_j \setminus \{v_i\} : v_i \in e_j, e_j \in \mathcal{E}\}$). The reason for multiset is that given subsets can be duplicated due to the nature of overlapping hyperedges (e.g., when we omit a node v_1 from $\{v_1, v_2, v_3\}$ and v_4 from $\{v_4, v_2, v_3\}$, remaining sets become identical).

We split the derivation into the node level. In addition, we let a subset of $\mathcal{Q}$ such that includes a node v_k as $\mathcal{Q}_k$. Then, for a node v_k, its gradient is computed as follows:

$$\sum_{q_j \in \mathcal{Q}} \frac{\exp\left(\boldsymbol{z}_k^T \left(\sum_{v_s \in q_j} \boldsymbol{z}_s\right)\right)}{\sum_{v_t \in \mathcal{V}} \exp\left(\boldsymbol{z}_t^T \left(\sum_{v_s \in q_j} \boldsymbol{z}_s\right)\right)} \times \left(\sum_{v_s \in q_j} \boldsymbol{z}_s\right) \tag{70}$$

$$+ \sum_{q_l \in \mathcal{Q}_k} \sum_{v_i \in \mathcal{V}} \frac{\exp\left(\boldsymbol{z}_i^T \left(\sum_{v_s \in q_l} \boldsymbol{z}_s\right)\right)}{\sum_{v_t \in \mathcal{V}} \exp\left(\boldsymbol{z}_t^T \left(\sum_{v_s \in q_l} \boldsymbol{z}_s\right)\right)} \boldsymbol{z}_i. \tag{71}$$

We define two more matrices to express the above equations in a simple matrix form. By assigning an index $k = \{1, \cdots, |\mathcal{Q}|\}$ to each element of $q_j \in \mathcal{Q}$, we define a binary matrix $\mathbf{Q} \in \mathbb{R}^{|\mathcal{Q}| \times |\mathcal{V}|}$ that represents $\mathcal{Q}$ as follows:

$$\mathbf{Q}_{ji} = \begin{cases} 1 & \text{if } v_i \in q_j, \\ 0 & \text{otherwise.} \end{cases}$$

In addition, we denote a score matrix $\mathbf{A} \in \mathbb{R}^{|\mathcal{Q}| \times |\mathcal{V}|}$ that models a probability of filling each node $v_i \in \mathcal{V}$ to each set $q_j \in \mathcal{Q}$, which is defined as follows:

$$\mathbf{A}_{ki} = \frac{\exp\left(\boldsymbol{z}_i^T \left(\sum_{v_s \in q_j} \boldsymbol{z}_s\right)\right)}{\sum_{v_t \in \mathcal{V}} \exp\left(\boldsymbol{z}_t^T \left(\sum_{v_s \in q_j} \boldsymbol{z}_s\right)\right)}. \tag{72}$$

By using $\mathbf{A}$ and $\mathbf{Q}$, we can express Eq (70) and (71) for all nodes as follows:

$$\left(\underbrace{\mathbf{Q}^T \mathbf{A}}_{\text{Eq (70) of all nodes}} + \underbrace{\mathbf{A}^T \mathbf{Q}}_{\text{Eq (71) of all nodes}} \right) \mathbf{Z}. \tag{73}$$

Finally, we express $(\partial \mathcal{L} / \partial \mathbf{Z})$ as follows:

$$\frac{\partial \mathcal{L}}{\partial \mathbf{Z}} = \left(-\mathbf{E} + \mathbf{Q}^T \mathbf{A} + \mathbf{A}^T \mathbf{Q}\right) \mathbf{Z}. \tag{74}$$

In addition, by using the chain rule and derivative of matrix multiplication, $\partial \mathcal{L} / \partial \mathbf{W}$ is derived as follows:

$$\frac{\partial \mathcal{L}}{\partial \mathbf{W}} = \mathbf{X}^T \left(-\mathbf{E} + \mathbf{Q}^T \mathbf{A} + \mathbf{A}^T \mathbf{Q}\right) \mathbf{X} \mathbf{W}. \tag{75}$$

We denote updated $\mathbf{W}$ as $\tilde{\mathbf{W}}$. To sum up, update rule of $\tilde{\mathbf{W}} := \mathbf{W} - \gamma \nabla_{\mathbf{W}} \mathcal{L}$ is written as follows:

$$\tilde{\mathbf{W}} := \left(\mathbf{I} + \gamma \mathbf{X}^T \left(\mathbf{E} - \mathbf{Q}^T \mathbf{A} + \mathbf{A}^T \mathbf{Q}\right) \mathbf{X}\right) \mathbf{W}. \tag{76}$$

Here, we denote k-th biggest singular values of $\tilde{\mathbf{W}}$ and $\mathbf{W}$ as $\tilde{\sigma}_k$ and σ_k, respectively.

Note that $\left(\mathbf{I} + \gamma \mathbf{X}^T \left(\mathbf{E} - \mathbf{Q}^T \mathbf{A} + \mathbf{A}^T \mathbf{Q}\right) \mathbf{X}\right)$ is a function of $\mathbf{X}$, $\mathcal{E}$, and $\mathbf{W}$. Thus, we denote this term as $g(\mathbf{X}, \mathcal{E}, \mathbf{W}) \in \mathbb{R}^{d \times d}$.

If we take a closer look at $g(\mathbf{X}, \mathcal{E}, \mathbf{W})\mathbf{W}$, $\tilde{\mathbf{W}}$ is a near-linear transformation of $\mathbf{W}$ itself[8]. In such a case, from the min-max characterization, the following inequality holds:

$$\tilde{\sigma}_k \leq \sigma_1' \times \sigma_k, \text{ where } \sigma_1' \text{ is the biggest singular value of a matrix } g(\mathbf{X}, \mathcal{E}, \mathbf{W}). \tag{77}$$

Eq (77) indicates that $\tilde{\sigma_k}$ is upper-bounded by the multiplication between the biggest singular value of $g(\mathbf{X}, \mathcal{E}, \mathbf{W})$ and σ_k. While it is not an exact equality, this result implies that the changed singular value is likely to be correlated with its previous singular value. Hence, small singular values are likely to grow slowly, similar to the case that is suggested by Jing et al. (2022), which may cause dimensional collapse.

C DATASETS

In this section, we provide details of the used datasets. In our experiments, we have utilized 11 hypergraph benchmark datasets. We have removed nodes that do not belong to any hyperedge, following Lee & Shin (2023). Data statistics of each dataset are reported in Table 4.

Source of each dataset. The sources of used datasets in this work are as follows:

- Cora, Citeseer, Pubmed, Cora-CA, and DBLP-P datasets are from the work of Yadati et al. (2019).

[8] It is not a perfect linear transformation, since a function $g(\cdot)$ also receives W as an input

Table 4: Statistics of datasets we have used in our experiments.

	Citeseer	Cora	Pubmed	Cora-CA	DBLP-P	DBLP-A	AMiner	IMDB	MN-40	20News	House
$\lvert\mathcal{V}\rvert$	1,458	1,434	3,840	2,388	41,302	2,591	20,201	3,939	12,311	16,242	1,290
$\lvert\mathcal{E}\rvert$	1,079	1,579	7,963	1,072	22,263	2,690	8,052	2,015	12,311	100	341
$\sum_{e\in\mathcal{E}}\lvert e\rvert$	3,453	4,786	34,629	4,585	99,561	6,201	32,028	9,560	61,555	65,451	11,843
# Classes	6	7	3	7	6	4	12	3	40	4	2
# Features	3,703	1,433	500	1,433	1,425	334	500	3066	100	100	2

- DBLP-A and IMDB datasets are from the work of Wang et al. (2019).
- AMiner dataset is from the work of Zhang et al. (2019).
- Mondelnet-40 (MN-40) dataset is from the work of Wu et al. (2015).
- 20Newsgroups (20News) dataset is from the work of Dua et al. (2017).
- House dataset is from the work of Chien et al. (2022).

Co-citation datasets. We utilize three co-citation datasets: Cora, Citeseer, and Pubmed. In these datasets, each node represents a publication and hyperedges represent sets of publications co-cited by particular publications. For example, if a particular publication has cited nodes (publications) v_i, v_j, and v_k, these nodes are grouped as a hyperedge $\{v_i, v_j, v_k\} \in \mathcal{E}$. Node features are bag-of-words of the corresponding publication. Node classes indicate categories of the publication.

Co-authorship datasets. We utilize four co-authorship datasets: Cora-CA, DBLP-P, DBLP-A, and AMiner. In Cora-CA, DBLP-P, and AMiner, each node represents a publication, and a set of publications that are written by a particular author is grouped as a hyperedge. Features are bag-of-words of the corresponding publication, and classes indicate categories of the publication. Conversely in DBLP-P, each node represents an author, and co-authors of a particular publication are grouped as a hyperedge. Node features are bag-of-words regarding the research keywords of the author. Node classes indicate the research area of the author.

Computer graphic datasets. We utilize one computer graphical dataset: Modelnet-40 (MN-40). In this dataset, each node represents a visual object, and hyperedges are synthetic hyperedges that have been created with a k-NN graph constructed according to the features of each data point, following Feng et al. (2019) and Chien et al. (2022). Node features are embeddings of each visual object obtained via GVCNN (Feng et al., 2018) and MVCNN (Su et al., 2015). Node classes indicate the categories of the corresponding visual object.

Movie-Actor dataset. We utilize one movie-actor dataset: IMDB. In this dataset, each node indicates a movie, and the filmography of a particular actor is grouped as a hyperedge. Node features are bag-of-words of the plot of the movie. Node classes indicate the genre of the movie.

News dataset. We utilize one news dataset: 20NewsGroups (20News). In this dataset, each node represents documents of 20 newsgroups and a set of documents containing a particular word is grouped as a hyperedge. Node features are TF-IDF representations of news messages. Node classes indicate the categories of the corresponding document.

Political membership dataset. We utilize one political membership dataset: House. In this dataset, each node represents a member of the US House of Representatives, and members belonging to the same committee are grouped as a hyperedge. Node features are created by adding noise to the one-hot encoded label vector, as suggested by Chien et al. (2022). Node classes indicate the political party of the representatives.

D Experimental Details

In this appendix section, we provide details of our experiments. We first describe the machines we have used in our experiments. Then, we provide details of baseline methods and implementations.

Table 5: Hyperparameter combination of HYPEBOY that shows the best validation accuracy on each dataset. $p_v \in [0, 1]$ indicates magnitude of feature augmentation, p_e indicates magnitude of topological augmentation, and $SSLepochs$ indicates the training epoch of hyperedge filling task.

	Citeseer	Cora	Pubmed	Cora-CA	DBLP-P	DBLP-A	AMiner	IMDB	MN-40	20News	House
p_v	0.2	0.4	0.0	0.4	0.0	0.1	0.2	0.3	0.4	0.2	0.4
p_e	0.9	0.9	0.5	0.8	0.6	0.9	0.6	0.9	0.5	0.5	0.8
SSL epochs	120	200	180	200	180	120	100	180	180	80	140

D.1 MACHINES

All experiments are conducted on a machine with NVIDIA RTX 8000 D6 GPUs (48GB memory) and two Intel Xeon Silver 4214R Processors.

D.2 DETAILS OF BASELINE METHODS

Neural networks. We utilize 10 supervised baseline models: MLP, HGNN (Feng et al., 2019), HyperGCN (Yadati et al., 2019), HNHN (Dong et al., 2020), three unified hypergraph networks, (UniGCN, UniGIN, UniGCNII) (Huang & Yang, 2021), AllSet (Chien et al., 2022), ED-HNN (Wang et al., 2023a), and PhenomNN (Wang et al., 2023b).

Graph SSL. In order to run two graph generative SSL methods, which are GraphMAE2 (Hou et al., 2023) and MaskGAE (Li et al., 2023), we transform the input hypergraph into a graph by using the clique expansion, which converts each hyperedge into a clique of a graph (Dong et al., 2020).

H-GD. One of our baseline methods H-GD directly extends the Group Discrimination method, an SSL technique designed on a graph (Zheng et al., 2022). We strictly follow the overall structure suggested by Zheng et al. (2022), while the feature augmentation and topology augmentation have been replaced into $\boldsymbol{\tau}_x$ and $\boldsymbol{\tau}_e$ that are described in Section 4.1, respectively.

D.3 DETAILS OF SETTINGS AND IMPLEMENTATIONS

Hyperedge prediction setting. Note that we need to create negative hyperedge samples to evaluate the performance of a model on the hyperedge prediction task. In our experiment, we have created negative hyperedge samples based on SNS (size negative samples) (Patil et al., 2020). Specifically, to create a negative hyperedge, we sample a size of the current hyperedge from the real-world hyperedge size distribution of the corresponding dataset. Then, we sample nodes uniformly at random and fill the corresponding hyperedge. In this manner, we create negative hyperedges with the same number of ground-truth hyperedges.

Feature reconstruction warm-up of HYPEBOY. As described in Section 4.4, before training an encoder HNN with HYPEBOY, we utilize a feature reconstruction process, which directly extends GraphMAE (Hou et al., 2022) to hypergraph structure. This process mitigates the encoder's over-reliance on the projection heads, improving the performance in downstream tasks (Section 5.3).

To this end, we first mask a certain portion of input node features with a learnable mask token. We have fixed the augmentation portion as 0.5 for all the cases. In addition, we augmentation the input hyperedge by using $\boldsymbol{\tau}_{\mathcal{E}}$, which is defined in Section 4.1. We have fixed the magnitude of augmentation p_e as 0.2 for all the cases. Then, we obtain node embeddings by using an encoder HNN. We again mask embeddings of nodes that have been masked at the input level by using another learnable mask. Subsequently, we obtain reconstructed features with an HNN decoder, which has an architecture that is the same as that of the encoder HNN. Finally, we utilize the cosine similarity between reconstructed features and original features as a loss, specifically, one minus cosine similarity. Specifically, we utilize UniGCNII (Huang & Yang, 2021) for encoder and decoder.

Projection heads of HYPEBOY. For projection heads (Section 4.2), we utilize a two-layer MLP model with a ReLU (Nair & Hinton, 2010) activation function for both node projection head f'_ϕ and set projection head f'_ρ. Note that these projection heads are updated via the hyperedge filling task together with an encoder HNN.

Table 6: Comparison between HYPEBOY without augmentation step (denoted by w/o Aug.) and HYPEBOY (denoted by w/ Aug.) in the node classification task under two protocols. The best performance is colored as a green. In most of the settings, HYPEBOY outperforms its variant.

Protocol	Method	Citeseer	Cora	Pubmed	Cora-CA	DBLP-P	DBLP-A	AMiner	IMDB	MN-40	20News	House
Fine tuning	w/o Aug.	53.5 (8.7)	58.6 (8.3)	75.5 (4.0)	62.9 (6.0)	87.8 (0.4)	79.7 (2.3)	33.9 (2.1)	47.2 (2.5)	90.7 (0.7)	77.5 (0.9)	69.9 (4.9)
	w/ Aug.	56.7 (9.8)	62.3 (7.7)	77.0 (3.4)	66.3 (4.6)	88.2 (0.4)	80.6 (2.3)	34.1 (2.2)	47.6 (2.5)	90.4 (0.9)	77.6 (0.9)	70.4 (4.8)
Linear evaluation	w/o Aug.	55.8 (9.0)	60.6 (7.3)	72.7 (3.4)	63.3 (4.6)	87.6 (0.5)	81.4 (2.5)	34.2 (2.7)	47.8 (2.0)	89.7 (1.9)	75.1 (1.6)	67.5 (1.6)
	w/ Aug.	59.6 (9.9)	63.5 (9.4)	75.0 (3.4)	66.0 (4.6)	87.9 (0.5)	81.2 (2.7)	34.3 (3.2)	48.8 (1.8)	89.2 (2.2)	75.7 (2.1)	69.4 (5.4)

Training details and hyperparameters. We utilize the Adam optimizer (Kingma & Ba, 2015) with a fixed weight decay rate of 10^{-6} to train all models. We fix the hidden dimension of all models and the dropout rate of them as 128 and 0.5, respectively. When training any neural network for downstream tasks, we train the model for 200 epochs, and for every 10 epochs, we evaluate the validation accuracy of the model. Then, we utilize the model checkpoint that yields the best validation accuracy to make a final evaluation of the model on the test dataset.

For a linear evaluation protocol of node classification, we utilize a logistic classifier, with a learning rate 10^{-3}. For a linear evaluation protocol of hyperedge classification, we utilize a two-layer MLP, with a learning rate of 10^{-3} and the dropout rate of 0.5.

Regarding hyperparameter tuning, for each model and dataset, we find the hyperparameter combination that gives the best validation performance. Then, with the selected hyperparameters, we train the model on a training dataset and evaluate the performance of the trained model on a test dataset.

For all the supervised models we have used, we tune the learning rate as a hyperparameter within $\{0.05, 0.01, 0.005, 0.001, 0.0005, 0.0001\}$. Moreover, especially for SOTA HNNs PhenomNN, we additionally tune their other hyperparameters. Specifically, along with the learning rate, we additionally tune λ_0 and λ_1 within $\{0, 1, 10\}$, which are weights of different message-passing functions, and α within $\{0, 1, 10\}$ which is a weight of node's own representation during encoding.

For all SSL baseline methods, we set a broader search space, which is as follows:

- TriCL (Lee & Shin, 2023): We tune their feature augmentation magnitude within $\{0.2, 0.3, 0.4\}$, hyperedge augmentation magnitude within $\{0.2, 0.3, 0.4\}$, and learning rate of an encoder within $\{0.01, 0.001, 0.0001\}$.
- HyperGCL (Wei et al., 2022): We tune learning rate of an encoder within $\{0.01, 0.001, 0.0001\}$, that of a generator $\{0.01, 0.001, 0.0001\}$, and weight of contrastive loss β within $\{0.5, 1, 2\}$.
- HGD, variant of GD (Zheng et al., 2022): We tune their feature augmentation magnitude within $\{0.2, 0.3, 0.4\}$, hyperedge augmentation magnitude within $\{0.2, 0.3, 0.4\}$, and learning rate of an encoder within $\{0.01, 0.001, 0.0001\}$.
- GraphMAE2 (Hou et al., 2023): We tune mask ratio within $\{0.25, 0.5, 0.75\}$ and learning rate of an encoder within $\{0.01, 0.001, 0.0001\}$.
- MaskGAE (Li et al., 2023) We tune degree loss weight α within $\{0.001, 0.002, 0.003\}$ and learning rate of an encoder within $\{0.01, 0.001, 0.0001\}$.

In addition, we set self-supervised learning epochs of the above methods as hyperparameters, searching within $\{50, 100, 150, \cdots, 450, 500\}$.

For HYPEBOY, we tune feature augmentation magnitude p_x within $\{0.0, 0.1, 0.2, 0.3, 0.4\}$, and hyperedge augmentaiton magnitude p_e within $\{0.5, 0.6, 0.7, 0.8, 0.9\}$. We have fixed the learning rate and training epochs of the feature reconstruction warm-up as 0.001 and 300, respectively. In addition, we first train an encoder with a feature reconstruction process for 300 epochs. Then, we train the encoder with the hyperedge filling, and the specific epoch is a hyperparameter searched within $\{20, 40, \cdots, 180, 200\}$. We report a hyperparameter combination of each dataset that shows the best validation accuracy in our fine-tuning experiment (Section 5.1) in Table 5.

E ADDITIONAL EXPERIMENTAL RESULTS

In this section, we present several experimental results that are omitted in the main paper.

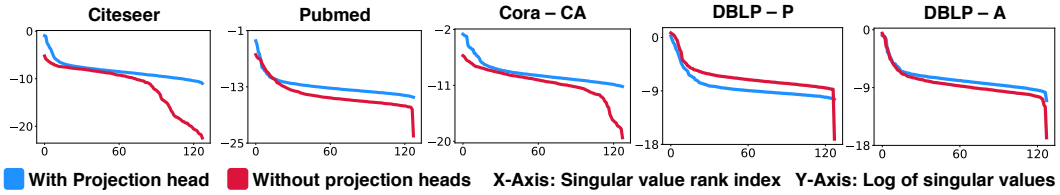

Figure 4: Analyzing dimensional collapse of HYPEBOY with/without projection heads on five benchmark datasets. While HYPEBOY does not suffer from dimensional collapse, its variant that does not utilize projection heads, suffers from this issue.

E.1 COMPARISON AGAINST HYPEBOY WITHOUT AUGMENTATION

As described in Section 4.1, augmentation (masking) has played a key role in various generative SSL methods in obtaining effective representations. Motivated by their findings, we have also adopted augmentation strategy $\boldsymbol{\tau}_x$ and $\boldsymbol{\tau}_e$ in HYPEBOY also. To demonstrate the effectiveness of augmentation, we have employed one variant of HYPEBOY, where the augmentation step is omitted. In other words, the input of a target HNN f_θ is always a clean feature and topology, $(\mathbf{X}, \mathcal{E})$. Then, we compare this variant with our proposed HYPEBOY, in the node classification task under fine-tuning protocol and linear evaluation protocol. As shown in Table 6, HYPEBOY outperforms its variant, which does not have an augmentation step in most of the datasets of both protocols. Thus, we can conclude that augmentation is crucial for mitigating the issue of over-emphasizing proximity information and creating effective representations.

E.2 DIMENSIONAL COLLAPSE ANALYSIS

In Section 4.2, we discuss the role of projection heads in terms of dimensional collapse: projection heads encourage an encoder HNN to avoid dimensional collapse. We further anlyze this phenomenon in five more benchmark hypergraph datasets: Citeseer, Pubmed, Cora-CA, DBLP-P, and DBLP-A. As shown in Figure 4, in all five datasets, we have verified that small singular values of embeddings that are created via HYPEBOY without projection heads drop to zero, empirically demonstrating that the dimensional collapse has occurred (red lines). Notably, such an issue has not been observed in HYPEBOY (blue lines).

E.3 ALIGNMENT AND UNIFORMITY ANALYSIS

In Section 4.3, we discuss the role of our design choice of $p_{(\mathbf{X},\mathcal{E},\Theta)}(\cdot)$ in promoting alignment and uniformity of representations. We further demonstrate this characteristic in five more benchmark hypergraph datasets: Citeseer, Pubmed, Cora-CA, DBLP-P, and DBLP-A. As shown in Figure 5, representations obtained from HYPEBOY achieve both uniformity (first column) and alignment (other columns) in most of the cases.

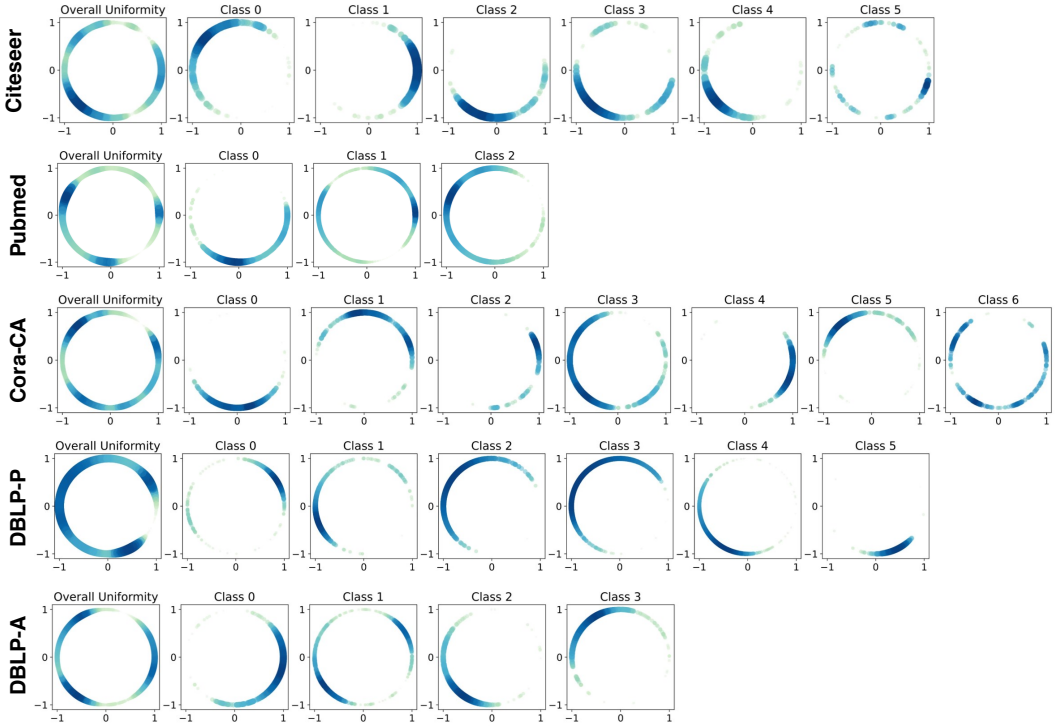

Figure 5: Analyzing alignment and uniformity of representations obtained via HYPEBOY. In most cases, representations obtained by HYPEBOY achieve both alignment and uniformity.